Low-Frequency Oscillation in Electric Railway Depot: A Comprehensive Review

Haitao Hu, *Senior Member, IEEE*, Yi Zhou, *Student Member, IEEE*, Xin Li, and Ke Lei

***Abstract*—The wide adoption of a new type of electric trains results in multiple frequency-scale instability problems, such as low-frequency oscillation (LFO), harmonic resonance, and harmonic instability. Among them, LFO has been commonly reported at electric railway depots with multiple-energized electric trains around the whole world, thus attracting widespread research attention. LFOs cause adverse effects on the system stability and protection infrastructure of both the traction network and electric trains. This article presents a comprehensive review of LFOs that consider both academic theoretical analysis and industrial engineering requirements. A unified mathematical model of the traction network and electric train is derived with a view to revealing the mechanism and factors that induce LFOs when these two systems interact. The article also draws deep insights from results of experimental measurements and industrial mitigation schemes already implemented in Chinese railway systems. A variety of mitigation techniques and recommendations based on theoretical principles and practical constraints are presented.**

***Index Terms*—Electric railway, elimination methods, low-frequency oscillation, stability analysis.**

I. Introduction

In RECENT years, the enormous rise in demand for transportation via high-speed/heavy-haul electric railways has motivated rapid development of modern electric trains. Although these trains have advantages which include excellent traction and environment-friendly performance, yet this circumstance also introduces new challenges in terms of poor power quality and instability to both the traction network and multiple electric trains that are powered by the networks [1]–[3]. Several low-frequency oscillation (LFO) incidents, from 1 Hz to several Hertz, have been reported in the literatures [4]–[6]. This oscillation phenomenon differs significantly from traditional power-angle and voltage instabilities in power systems [7]. The LFO is due to the interaction between the traction network and the power-electronics interfaces in electric trains. As a result, the LFO requires the small-signal stability analysis [8]. Furthermore, this oscillation has the greatest effects on the traction network and is rapidly attenuated through traction transformers when it flows to the utility grid.

The earliest reported LFO phenomenon occurred in 1996 in Norway, where a rotating converter was adopted in a traction substation (TSS), when introducing the NSB locomotive class EL18 [9]. Subsequently, in Germany, Sweden, and Norway, the traction network has been interfaced with rotating converters that transform three-phase utility power into single phase to power the catenary network [10]. The electromechanical characteristics of rotating converters have been identified as the main cause of the LFO [11].

However, for other electric railway systems, the mechanism of LFO remains unclear. Most of these systems rely on the V/v- or Scott- connection traction transformers instead of rotating converters. More recently, from 2008 to 2016, LFOs have been observed in increasing frequency at railway depots in China, Switzerland, and France [12], [13]. These oscillations result in system protection malfunction and increase the unscheduled downtime of electric trains.

As a result of the aforedescribed problems, a variety of techniques to solve this problem has been reported. Some of these are field test and data analysis [2], [14], time-domain simulation [4], [15]–[17], hybrid time-domain, and frequency-domain theoretical analysis (i.e., eigenvalue method [3], [8] and frequency domain analysis [18]–[21]), etc.

The field test method involves the intentional excitation of the LFO phenomenon by simulating the causal conditions. According to the analysis of measurement data, the factors and conditions that induce LFO are unfolded. However, field tests have been limited in finding the mechanism. An alternative method is time-domain simulation by software such as MATLAB, PSCAD, or Simpow [15]–[17]. For example, the stability of the train-network system with a long catenary network and one train was simulated in PSCAD. This investigation revealed that the chosen topology for rectifier bridges could affect the system's stability significantly [16].

Because the LFO is a type of small-signal instability caused by the interaction between a traction network and electric trains [8]. There are two categories of theoretical methods for system-level LFO analysis, i.e., eigenvalue analysis based on the state-space model in the time-domain [22]–[24], and impedance-based analysis in the frequency-domain [25]–[27]. The superior features of the former approach are the identification of the oscillatory modes, damping ratio, and sensitivity index of the system variables [28]. However, due to the wide timescale dynamics of

Manuscript received October 30, 2019; revised February 1, 2020 and April 6, 2020; accepted May 15, 2020. Date of publication May 29, 2020; date of current version September 4, 2020. This work was supported in part by the National Key Research and Development Program of China under Grant 2017YFB 1200802 and in part by the National Natural Science Foundation of China under Grant NSFC 51677154. Recommended for publication by Associate Editor Y. Yang. *(Corresponding author: Haitao Hu.)*

The authors are with the School of Electrical Engineering, Southwest Jiaotong University, Chengdu 610031, China (e-mail: hht@swjtu.edu.cn; zhouyipower@163.com; lixin3129@163.com; leike_swjtu@163.com).

Color versions of one or more of the figures in this article are available online at https://ieeexplore.ieee.org.

Digital Object Identifier 10.1109/TPEL.2020.2998702

converters, the electromagnetic dynamics of the system must be included in the state-space model. This significantly increases the system order and thus requires high computational resources [29], [30]. The later approach extracts the dynamics of the converters at their terminals by using frequency-domain transfer functions and then translates them to electric impedances. This makes the model for system stability amenable to investigation by means of circuit theory [26], [29]. The main superior aspect of the impedance-based methods lies in black-box modeling, i.e., measurements without the prior knowledge of detailed system parameters [31].

Moreover, many methods, in addressing the linearization of power electronic converters are also classified into two categories based on the operation points or trajectories. These are linear time invariant (LTI) models [32] and linear time-periodic models [33], [34]. The averaged-impedance model is a kind of LTI model that is based on state-space averaging, and it is accurate in identifying the low-frequency instability issues when the frequency is below the Nyquist frequency $(f_{sw}/2)$, e.g., the LFO or subsynchronous oscillation. The *dq* impedance modeling [35] and harmonic linearization [36] are two main approaches to build the averaged-impedance model for an ac systems. The *dq* impedance modeling transfers the ac system to a *dq*-frame and then adopts small-signal linearization at dc steady-state operation point. Moreover, the harmonic linearization adds an assumed perturbation ac signal and then derives the response signal of the disturbance based on the harmonic balance principle and small-signal linearization. In addition, when the frequency of the instability problem is above $f_{sw}/2$, the dynamic behavior of the pulsewidth modulation (PWM) should be considered [37]. Harmonic state space is applicable for this purpose and it is a kind of multiple frequency model [34]. Additionally, when the LFO occurs, the oscillation waveforms contain predominantly $f_0 \pm f_{\rm osc}$ components instead of oscillatory component $f_{\rm osc}$ [21] (where f_0 is the fundamental frequency of the power system and $f_{\rm osc}$ is the oscillatory frequency of the dc-link voltage). Thus, a unified impedance model has been proposed to solve this phenomenon defined as a frequency coupling issue [38], which is a special case of the multiple frequency model.

The LFO phenomenon arises from the interaction between controllers of multiple electric trains and different combinations of network electric components and parameters [5], [8]. This article provides a wide range of combinations of the electric parameters to model the traction network. A detailed small-signal model of the electric train considering a complicated controller is derived together. Therefore, this article contributes to the subject of the LFO phenomenon in electric railways. The main contributions are the identification of the traction network and the electric trains as an equally interactive system, comprehensive discussion of the features of the phenomena, formation mechanism, and eliminating approaches based on a large amount of operational data from actual railway systems. Furthermore, the article elaborates on suggested approaches toward eliminating LFO.

The remainder of this article is organized as follows. Section II surveys typical field LFO cases that provide details on their features and summaries of the LFO events. Modeling of the train-network system and modeling of the electric trains are discussed in detail in Section III. Section IV presents the mechanism and influential factors of the LFO data analytically and mathematically. In Section V, the suppression methods of LFO are discussed from the onboard and traction network aspects. The standards for addressing LFOs are discussed in Section VI. Finally, Section VII concludes the article.

TABLE I
LFO CASES WITH ROTARY CONVERTER

No.	$f_{\rm osc}$/Hz	f_0/Hz	Time	Located
1	1.6	16.67	2007	Norway
2	1.2	25	1997	America
3	1.6	16.67	1991	Germany
4	1.9	16.67	1991	Germany

Fig. 1. Multiple electric trains in a railway depot under LFO experiments.

II. LFO PHENOMENA IN ELECTRIC RAILWAYS

A. LFO Field Tests

There are two types of LFO scenarios depending on the intervention of the rotary frequency converter. Some electrified railways in Norway, Sweden, Germany, and Switzerland have adopted the rotary frequency converter as the power supply solution [11]. Table I presents a survey of this type of LFO cases over the whole world. The typical oscillatory frequency $f_{\rm osc}$ is approximately 10–30% of the respective power system's fundamental frequency f_0. The rotary converter, which is used for the power supply mode variations in TSSs, excites oscillations, i.e., by active power changes in the 16⅔ Hz ac railway system.

The second scenario of LFO phenomena occurs mainly in a rail depot, where multiple trains are preparing for operation and located far from the TSS [14]. Multiple trains in the rail depot shown in Fig. 1 are energized simultaneously by the pantographs, leading to a 0.6–7 Hz network voltage oscillation. As a result, the four-quadrant converters (4QCs) of the electric trains are locked and shut down. Alternatively, different types of electric trains in different railway systems have experienced similar LFOs in their rail depots, although the frequencies were different. Some cases of LFO phenomenon that involve a rail depot without a rotary converter are listed in Table II.

Fig. 2 shows the measurements of the LFO in a railway depot with an increasing number of electric trains connected to the traction network. The voltage and current waveforms are seen to oscillate when the sixth train is connected [see Fig. 2(b)].

TABLE II
LFO CASES WITHOUT ROTARY CONVERTER

No.	f_{osc}/Hz	f_0/Hz	Time	Case
1	5	50	2008	Thionville, France [10]
2	7	50	2006	Siemens test, Germany[10]
3	3	25	2006	Washington, DC, USA [10]
4	5	16.67	1995	Zurich, Switzerland [10]
5	2~4	50	2008-01	Hudong Depot, HX_D1
6	5	50	2010-01	Shanghai Nanxiang, CRH_1
7	5	50	2010-09	Qingdao Depot, CRH_5
8	0.6~2	50	2015-12	Xuzhou Hub, HX_D2B
9	6~7	50	2011-11	Shanhaiguan Hub, HX_D3B

Note: Locations in No. 5–9 are in China.

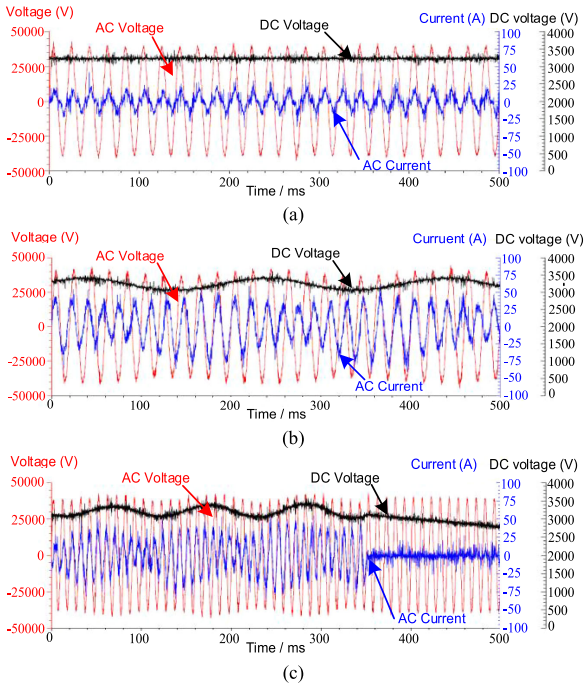

Fig. 2. Measured voltage and current waveforms with different train numbers: (a) less than 5 trains; (b) 6 trains; (c) 7 trains [14].

Consequently, the oscillatory voltage and current waveforms contain a significant low-frequency envelope. Thus, it is called a low-frequency oscillation. It is worthwhile to note that traction lockout arose in the tested trains, owing to the voltage and current fluctuating intensely from 350–500 ms. This indicates that multiple electric trains may easily destabilize the traction network and change the oscillatory frequency.

Furthermore, to investigate the oscillatory frequencies and modes, field tests were done in another Chinese railway depot in January 2016. When seven or eight trains were connected to the traction network, the voltage and current waveforms of the traction network started to oscillate. A schematic diagram of the actual test scenario is shown in Fig. 3. With the number of trains increasing, the voltage and current waveforms in different positions (TSS, switching station, and train) are recorded. Obviously, three different oscillatory modes can be involved: 1) periodic fluctuation approximately 0.6 to 0.8 Hz; 2) periodic fluctuation around approximately 2 Hz; and 3) irregular fluctuation (unstable oscillation). Among these, irregular fluctuation contributes

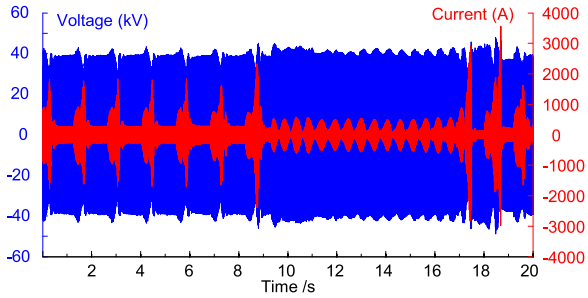

Fig. 3. Actual test and waveforms with three different oscillation/instable modes. 0–9 s, the oscillation is increasing amplitude; 9–17 s, the oscillation is attenuated and equally oscillation, it is turned instability after 17 s.

to the worst situation of current magnitude amplification (max. 3600 A).

B. LFO Features and Adverse Impacts

Experiences from the China's railway system show that the critical number of trains leading to the LFO is approximately 6–8. This is further dependent on the grid strength and train type. It is noteworthy that the values of the current are usually small, so the trains work under light-loading condition (low-power operation mode) [21]. Moreover, with increasing train numbers, the relative strength of the traction network correspondingly becomes weaker. Hence, an LFO occurs easily under the condition of a weak network and multiple electric trains.

1) When an LFO occurs in an ac railway traction power system, the instantaneous value envelopes of the line voltage, current, and dc-link voltage in the train-network system all show a low-frequency (0.6–7Hz) fluctuation with constant amplitude and frequency.
2) The presence of an LFO is related to the number of trains. The magnitude of the fluctuation is directly proportional to the number of trains. Alternatively, the weakness of the traction network system can be also regarded as increasing operation number of the electric trains.
3) LFO usually occurs under special loading conditions of the train-network system. For instance, in China's railway systems, this circumstance occurs when multiple trains are housed at the rail depot but remain connected to the traction network to power auxiliary loads (light-loading). The auxiliary system draws power directly from the dc-link through the main 4QC. No LFO occurs when the auxiliary system draws power from the auxiliary winding of traction transformers, because the 4QC is not working.

The field tests also reveal that during the LFO, the direction of the power changes periodically [13]; thus the outer voltage loop and the inner current loop of the traction converter fail to reach the desired references. Therefore, the LFO, occurring under special working conditions, such as the light-loading condition, could seriously deteriorate the system's stability and dynamic performance.

Some adverse impacts of such LFO phenomenon on the normal operations of the electric railways include:

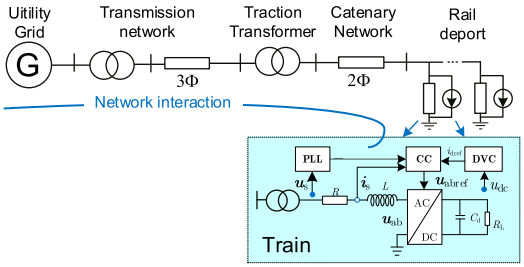

Fig. 4. Equivalent circuit of the electric railway system.

1) For instance, an LFO occurred at Qingdao and Hudong depots in China [39] , the oscillatory voltage exceeded 40 kV, setting off the operation of the power protection system. This resulted in power outage and interruption in services.
2) Voltage and current distorted the waveforms and generate continuous overcurrent (>3 kA), as shown in Fig. 3. These create potential damage to the onboard IGBT of the electric train and insulation breakdown of the network equipment.
3) A low-frequency component modulated to the fundamental-frequency voltage/current rapidly leads to the saturation state of the iron cores of the traction and onboard transformers [40]. There is also a resulting audible noise at the same low frequency. In addition, the low-frequency component causes higher power losses, temperature rise, and mechanical vibration in traction transformers.

III. Modeling of the Train-Network System

To investigate the mechanism of LFO and reveal different features of the field phenomena, it is required to identify the interaction between the traction network and the electric trains. First, the detailed models of two parts are discussed in this section.

The traction network system has three main constituents, i.e., the utility grid, TSS, and catenary network. Transmission/distribution lines interconnect these stages. For LFO analysis, the distributed capacitance of the transmission lines and the catenary network can be neglected in the low-frequency range. Thus, the impedance of the traction network can then be equivalent to a series circuit of resistor and inductor as seen from the trains (shown in Fig. 4.)

Moreover, the electric train has 4QCs, dc-link voltage loop, traction inverter, traction motor, and auxiliary system. During the operational state, since inverters and induction motors do not operate when trains are energized in the rail depot, they are neglected, and the auxiliary system is equivalent to a large resistor.

A. Modeling of the Traction Network

The equivalent circuit of the traction network can be simplified to a series of impedances of different electrical components. The detailed parameters are listed in Table III along with different combinations of possible electrical parameters, which are beneficial in understanding the mechanism of network variables.

1) Equivalent Impedance of the Utility Grid: At the point of connection to the utility grid in the TSS, the equivalent impedance of the power system is

$$X_u = \frac{U_g^2}{S_{\rm SC}}, \quad R_u = \frac{1}{K} \times \frac{U_g^2}{S_{\rm SC}} \tag{1}$$

where U_g is the rated voltage of the utility, $S_{\rm SC}$ is the rated capacity of the utility grid equipment connected to the TSS, and K is reactance resistance ratio. The 110-kV utility grid usually connects to a conventional railway, which has adopted the direct-supply catenary and its feeder catenary. On the other hand, a 220-kV utility voltage is powered for high-speed railways, which usually adopt the AT catenary system. Universal cases of utility grid are listed in Table III.

2) Equivalent Impedance of the TSS: The equivalent impedance of the TSS consists of two components: the impedance of traction transformer R_T, X_T, and that of catenary R_{Line}, X_{Line}. Here taking the V/x-mode traction transformer as an example, R_T, X_T are expressed as

$$R_T = \frac{P_k}{S_T} \times \frac{U_B^2}{S_T}, X_T = \frac{U_k\%}{100} \times \frac{U_B^2}{S_T} \tag{2}$$

where R_T and X_T are the resistance and reactance, P_k, U_B, S_T, and $U_k\%$ are the short-circuit loss, secondary-side voltage, rated capacity, and short-circuit voltage percentage of the traction transformer, respectively.

3) Equivalent Impedance of the Catenary Network: The catenary network, including the AT mode (i.e., 2×25kV), direct power supply mode (i.e., 1×25kV, DPS) and DPS with a negative line has different line impedances and associated angles adopted in protection applications. The impedance is relevant to the distance of the catenary and the power supply mode of substations. The ATs placed in ATS and SP can be neglected from the LFO analysis because their linkage impedances have a limited effect on the input impedance from the electric train [41]. Therefore, the input impedance, viewed from the electric train can be expressed as

$$R_{Line} = \frac{1}{2} l \times r_i \cos\varphi_i, X_{Line} = \frac{1}{2} l \times r_i \sin\varphi_i \tag{3}$$

where l is the length of the catenary lines. $r_i\angle\varphi_i$ is unit impedance per kilometer of three catenary modes, $0.18\angle75^{\rm o}$, $0.5\angle70^{\rm o}$, and $0.32\angle73^{\rm o}$, respectively. The coefficient 1/2 in (3) represents the double-line traction network mode.

4) Equivalent Impedance of the Whole Traction Network: It is necessary to transfer the three-phase impedance to a single-phase catenary network depending on the different connections of the traction transformers. The equivalent circuit of the traction network connected to the V/x-mode traction transformer and the corresponding circuit in α-phase are presented in Fig. 5. Z_α represents the equivalent impedance on the secondary side of the V/x transformer $Z_\alpha = 2Z_T$. Similarly, we can obtain the equivalent impedances of the other transformers [42].

The three-phase power grid, through different connections of traction transformers, can be transferred to the single-phase catenary network in this way.

TABLE III
LIST OF THE CASE STUDIES AND THEIR PARAMETERS FOR THE TRACTION NETWORK OF INTEREST

Case No.	*Utility Grid*		*Traction Transformer*		*Catenary Network*		Total impedance @ 27.5kV (Ω)	R_s (Ω)	R_s/X_s	SCR$_t$ (n=7, p=10)
	U_g (kV)	S_{SC} (GVA)	S_T (MVA)	U_k%	$r_i\angle\varphi_i$ (Ω/km)	l (km)				
1	110	0.3	31.5	10.5	0.5∠70°	25	16.19	2.72	0.17	1.07
		0.5					14.18	2.58	0.19	1.23
		1					12.67	2.48	0.20	1.37
		2					11.92	2.43	0.21	1.46
		5					11.47	2.40	0.21	1.51
2	220	1	31.5	10.5	0.32∠73°	25	10.49	1.51	0.15	1.66
		2					9.73	1.46	0.15	1.78
		5					9.28	1.43	0.16	1.87
		10					9.13	1.42	0.16	1.90
		20					9.05	1.42	0.16	1.92
3	220	5	20	8.4	0.32∠73°	25	10.63	1.79	0.17	1.63
			31.5	8.4			8.29	1.43	0.18	2.10
				10.5			9.28	1.43	0.16	1.87
				12			10.00	1.43	0.15	1.74
			40	10.5	0.18∠75°		6.49	0.75	0.12	2.68
				12			7.05	0.75	0.11	2.46
			50	8.4			5.07	0.70	0.14	3.43
				12			6.15	0.70	0.11	2.83
				14			6.75	0.70	0.10	2.57
			63	12			5.40	0.66	0.12	3.32
			80	12			4.79	0.64	0.14	3.63
				14			5.16	0.64	0.13	3.36
			126	14			4.20	0.62	0.15	4.13
4	220	5	31.5	10.5	0.5∠70°	10	7.78	1.12	0.15	2.23
						20	10.23	1.97	0.20	1.70
						30	12.71	2.83	0.23	1.37
					0.32∠73°	10	6.91	0.73	0.11	2.51
						20	8.50	1.20	0.14	2.05
						30	10.07	1.67	0.17	1.72
					0.18∠75°	10	6.23	0.50	0.08	2.79
						20	7.12	0.73	0.10	2.44
						30	8.01	0.96	0.12	2.17

When the train (or load) locates only in phase-α, the equivalent impedance of the TSS is

$$Z_g = R_s + jX_s = \frac{2}{k^2}(R_u + jX_u) + 2(R_T + jX_T) + (R_{Line} + jX_{Line}) \tag{4}$$

where *k* represents the transformation ratio of the traction transformer. Because the capacitance in the traction network can be neglected in the low-frequency range, the reactance is made equivalent to a pure inductance L_s. Therefore, from (1)–(4), the impedance matrix of the traction network in the *dq*-frame can be expressed as

$$\mathbf{Z}^g_{dq}(s) = \begin{bmatrix} R_s + sL_s & -\omega_0 L_s \\ \omega_0 L_s & R_s + sL_s \end{bmatrix} \tag{5}$$

where the superscript "g" represents the traction network and $L_s = X_s/(2\pi f_0)$.

TABLE IV
PARAMETERS OF TRAIN-NETWORK SYSTEM

Parameter	Symbol	Value
AC voltage of the 4QC	u_s	1770V
AC current of the 4QC	i_s	7.32A
DC-link voltage of the 4QC	u_{dc}	3600V
Fundamental frequency	f_0	50 Hz
Load resistor of the 4QC	R_L	1000Ω
Input inductor of the 4QC	L	5mH
DC-link capacitor of the 4QC	C_d	9mF
SOGI parameters	K_s, K	K_s=1, K=1
PLL control parameters	K_{pPLL}, K_{iPLL}	K_{pPLL} = 0.012, K_{iPLL} = 0.09
CC control parameters	K_{pC}, K_{iC}	K_{pC} = 1.57, K_{iC} = 4.93
DVC control parameters	K_{pV}, K_{iV}	K_{pV} = 0.49, K_{iV} = 6.79
Switch frequency	f_{sw}	500Hz
Sampling frequency	f_{sa}	1000Hz
Train quantity	n	7
Paralleled 4QC of one train	p	10
Utility Grid	U_g, K	220kV, 15
Traction Transformer	S_T, U_k%, P_k	31.5MVA, 10.5, 160kW
Catenary Network	l, $r\angle\varphi_l$	25km, 0.32∠73°Ω

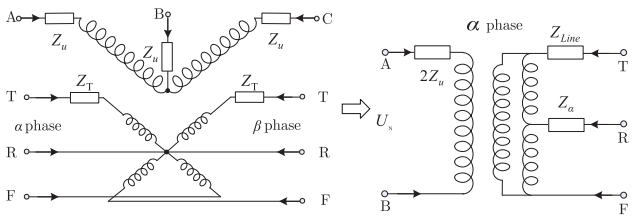

Fig. 5. Equivalent circuit of the traction transformer, where Z_u, Z_T, and Z_α are impedance of the utility grid, the single-phase impedance of the traction transformer, and the equivalent impedance in the second side of the V/x traction transformer, respectively.

Remark 1: The traction network is equivalent to a series of impedances and is combined to study the LFO problems. Almost all combination of main electric components forms the potential impedance or X_s/R_s values. The proportion of each component also represents the participation factor of the resulting LFO.

B. Modeling of the Electric Train

Electric trains normally adopt a voltage source PWM rectifier. The phase-locked loop (PLL) is used to capture the phase of the grid voltage and then achieve the synchronization between the ac voltage and ac current [43]. In addition, direct power control can obtain the synchronization current reference directly without PLL [44]. In this article, the voltage synchronization method is mainly considered in the modeling.

There are different topologies of the onboard main circuit. Among them, in a tractive unit, are single two-level, three-level, interlaced two-level converters. The three-level converter can be equivalent to the interlaced two-level converter when the phase difference of the carriers of the two converter is 180° [45]. In

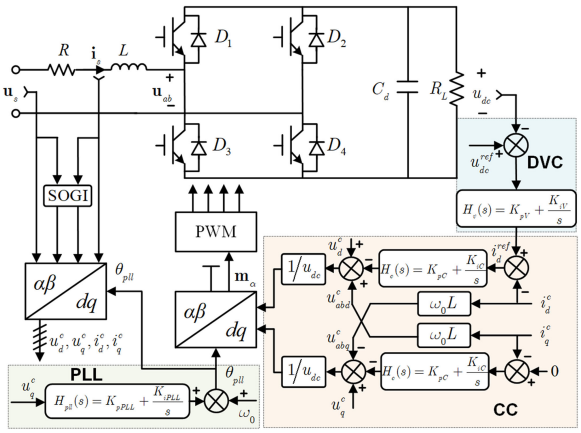

Fig. 6. Circuit and control system of the four-quadrant converter.

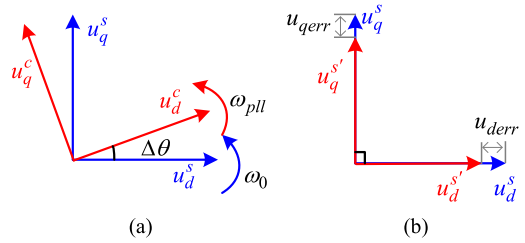

Fig. 7. Relationships among different *dq*-frames. (a) System *dq*-frame and controller *dq*-frame. (b) Ideal system *dq*-frame and actual system *dq*-frame.

the dual interleaved converters, each converter has the same controller structure but different carriers with phase shifting. Parallel converters with asynchronous carriers can cause harmonic resonance and instability due to the sideband harmonics produced by the pulsewidth modulator (PWM) [46]. However, in the low-frequency range, their PWM processes are equivalent to the average model. Therefore, the total impedance of the different trains can be simplified as the parallel result of 4QC with different numbers. One simplified converter is shown in Fig. 6.

In Fig. 6, the controller of the 4QC includes PLL, current controller (CC), and dc-link voltage controller (DVC). The CC is realized in *dq*-frame with a PI controller. The point of common coupling (PCC) voltage space vector and current space vector are $\mathbf{u}_s = [u_d\, u_q]^T$ and $\mathbf{i}_s = [i_d\, i_q]^T$, respectively. The modulation voltage space vector is $\mathbf{u}_{ab} = [u_{abd}\, u_{abq}]^T$.

Remark 2: Different topologies of the train's converters can be simplified as a set of parallel simple two-level converters that are modeled in the small-signal averaged model. In the low-frequency range, this assumption is necessary to handle different types of trains if we do not consider the impact of the PWM.

1) Modeling of Constructing Virtual β-Component in the Single-Phase Converter: First, in both single-phase and three-phase converters, due to the dynamic performance of the PLL, the converter has two *dq*-frames: one is the system *dq*-frame (labeled superscript "*s*"), and the other is the controller *dq*-frame (labeled superscript "*c*") [35]. The relationship between two *dq*-frames is shown in Fig. 7(a).

For the balanced three-phase system, three-phase voltages can be transferred to the two-phase static reference frame ($\alpha\beta$) by the Clarke's transformation, which can construct two components whose amplitudes are equal at any frequency. However, for the single-phase system, a virtual β component must be constructed to achieve Park's transformation by some methods, such as a T/4 delay, second-order generalized integrator (SOGI), all-pass filter, etc., [47]. In general, in the nonfundamental frequency, the virtual β-component generated by these methods has some phase or amplitude error compared with the ideal β-component, which will cause some errors in Park's transformation [5]. Therefore, the system *dq*-frame of the single-phase system is then divided as an ideal system *dq*-frame (labeled superscript "*s*") and actual system *dq*-frame (labeled superscript "*s*′"). The ideal system *dq*-frame is transferred by the ideal β component and the actual system *dq*-frame is transferred by the virtual β component. The relationship between the two system *dq*-frames is shown in Fig. 7(b).

In the frequency domain, the transfer matrices of the voltage and current between two system *dq*-frames can be expressed as

$$\begin{bmatrix}\Delta u_d^{s'}\\ \Delta u_q^{s'}\end{bmatrix} = \underbrace{\frac{1}{2}\begin{bmatrix}A_u(s)\ B_u(s)\\ -B_u(s)\ A_u(s)\end{bmatrix}}_{\mathbf{H}_{udq}(s)}\begin{bmatrix}\Delta u_d^{s}\\ \Delta u_q^{s}\end{bmatrix} \tag{6}$$

$$\begin{bmatrix}\Delta i_d^{s'}\\ \Delta i_q^{s'}\end{bmatrix} = \underbrace{\frac{1}{2}\begin{bmatrix}A_i(s)\ B_i(s)\\ -B_i(s)\ A_i(s)\end{bmatrix}}_{\mathbf{H}_{idq}(s)}\begin{bmatrix}\Delta i_d^{s}\\ \Delta i_q^{s}\end{bmatrix} \tag{7}$$

where

$$\begin{cases} A_u(s) = \left[\frac{1}{2}H_{\alpha u}(s+j\omega_0) + \frac{j}{2}H_{\beta u}(s+j\omega_0)\right] + \\ \qquad \left[\frac{1}{2}H_{\alpha u}(s-j\omega_0)\frac{j}{2}H_{\beta u}(s-j\omega_0)\right] \\ B_u(s) = \left[\frac{j}{2}H_{\alpha u}(s+j\omega_0) - \frac{1}{2}H_{\beta u}(s+j\omega_0)\right] + \\ \qquad \left[\frac{-j}{2}H_{\alpha u}(s-j\omega_0) - \frac{1}{2}H_{\beta u}(s-j\omega_0)\right] \end{cases}$$

$$\begin{cases} A_i(s) = \left[\frac{1}{2}H_{\alpha i}(s+j\omega_0) + \frac{j}{2}H_{\beta i}(s+j\omega_0)\right] + \\ \qquad \left[\frac{1}{2}H_{\alpha i}(s-j\omega_0) - \frac{j}{2}H_{\beta i}(s-j\omega_0)\right] \\ B_i(s) = \left[\frac{j}{2}H_{\alpha i}(s+j\omega_0) - \frac{1}{2}H_{\beta i}(s+j\omega_0)\right] + \\ \qquad \left[\frac{-j}{2}H_{\alpha i}(s-j\omega_0) - \frac{1}{2}H_{\beta i}(s-j\omega_0)\right]. \end{cases}$$

Equations (6) and (7) can be used to analyze the impact of any method for constructing the virtual β-component on the impedance if the transfer functions $H_\alpha(s)$ and $H_\beta(s)$ are known.

2) Modeling of the PLL: From Fig. 6, the transfer function of the PLL is derived as

$$\Delta\theta = \underbrace{\frac{H_{pll}(s)}{s + u_d^0 H_{pll}(s)}}_{G_{pll}(s)}\Delta u_q^{s'}. \tag{8}$$

The relationships of the voltage space vector, the current space vector, and the modulation voltage space vector between the actual system *dq*-frame and the controller *dq*-frame are respectively expressed as follows:

$$\begin{bmatrix}\Delta u_d^c\\ \Delta u_q^c\end{bmatrix} = \underbrace{\begin{bmatrix}1 & 0\\ 0 & 1 - u_d^0 G_{pll}(s)\end{bmatrix}}_{\mathbf{G}_{upll}(s)}\begin{bmatrix}\Delta u_d^{s'}\\ \Delta u_q^{s'}\end{bmatrix} \tag{9}$$

$$\begin{bmatrix}\Delta i_d^c\\ \Delta i_q^c\end{bmatrix} = \underbrace{\begin{bmatrix}0 & i_q^0 G_{pll}(s)\\ 0 & -i_d^0 G_{pll}(s)\end{bmatrix}}_{\mathbf{G}_{ipll}(s)}\begin{bmatrix}\Delta u_d^{s'}\\ \Delta u_q^{s'}\end{bmatrix} + \begin{bmatrix}\Delta i_d^{s'}\\ \Delta i_q^{s'}\end{bmatrix} \tag{10}$$

$$\begin{bmatrix}\Delta u_{abdref}^c\\ \Delta u_{abqref}^c\end{bmatrix} = \begin{bmatrix}\Delta u_{abdref}^s\\ \Delta u_{abqref}^s\end{bmatrix} - \underbrace{\begin{bmatrix}0 & -u_{abqref}^0 G_{pll}(s)\\ 0 & u_{abdref}^0 G_{pll}(s)\end{bmatrix}}_{\mathbf{G}_{dpll}(s)}\begin{bmatrix}\Delta u_d^{s'}\\ \Delta u_q^{s'}\end{bmatrix} \tag{11}$$

where the superscript "0" means the steady-state value.

3) Modeling of the DC-Link Voltage Loop: The dc-link voltage loop is used to keep the dc-link voltage stable and provides the reference signal for the current controller. In Fig. 6, the disturbance of the reference signal of the *d*-axis current is expressed as follows:

$$\Delta i_d^{\text{ref}} = -H_v \Delta u_{\text{dc}}. \tag{12}$$

According to the principle of power conservation, and neglecting the power losses in the rectifier switches, the dc-link voltage disturbance can be transformed to ac side in the ideal system *dq*-frame as follows:

$$\Delta u_{\text{dc}} = \underbrace{\begin{bmatrix}G_1(s)\ G_2(s)\end{bmatrix}}_{\mathbf{G}_i(s)}\begin{bmatrix}\Delta i_d^s\\ \Delta i_q^s\end{bmatrix} + \underbrace{\begin{bmatrix}G_3(s)\ G_4(s)\end{bmatrix}}_{\mathbf{G}_v(s)}\begin{bmatrix}\Delta u_d^s\\ \Delta u_q^s\end{bmatrix} \tag{13}$$

where

$$G_1(s) = \frac{0.5u_d^0}{sC_d u_{dc}^0 + u_{dc}^0/R_L}, G_2(s) = \frac{0.5u_q^0}{sC_d u_{dc}^0 + u_{dc}^0/R_L}$$

$$G_3(s) = \frac{0.5i_d^0}{sC_d u_{dc}^0 + u_{dc}^0/R_L}, G_4(s) = \frac{0.5i_q^0}{sC_d u_{dc}^0 + u_{dc}^0/R_L}.$$

4) Modeling the Current Loop and Modulation Block: The current loop provides the reference signal of the modulation voltage. The reference signal of the modulation voltage can be expressed as

$$\begin{bmatrix}\Delta u_{abdref}^c\\ \Delta u_{abqref}^c\end{bmatrix} = \begin{bmatrix}\Delta u_d^c\\ \Delta u_q^c\end{bmatrix} - \mathbf{H}_i(s)\begin{bmatrix}\Delta i_d^{ref} - \Delta i_d^c\\ \Delta i_q^{\text{ref}} - \Delta i_q^c\end{bmatrix} + \underbrace{\begin{bmatrix}0 & \omega_0 L\\ -\omega_0 L & 0\end{bmatrix}}_{\mathbf{G}_{\omega L}}\begin{bmatrix}\Delta i_d^c\\ \Delta i_q^c\end{bmatrix} \tag{14}$$

where $\mathbf{H}_i(s) = \begin{bmatrix}H_c(s) & 0\\ 0 & H_c(s)\end{bmatrix}$.

According to circuit theory, in the ideal system *dq*-frame, the actual modulation voltage can be expressed as

$$\begin{bmatrix}\Delta u_{abd}^s\\ \Delta u_{abq}^s\end{bmatrix} = \begin{bmatrix}\Delta u_d^s\\ \Delta u_q^s\end{bmatrix} - \underbrace{\begin{bmatrix}R + sL & -\omega_0 L\\ \omega_0 L & R + sL\end{bmatrix}}_{\mathbf{G}_{rl}(s)}\begin{bmatrix}\Delta i_d^s\\ \Delta i_q^s\end{bmatrix}. \tag{15}$$

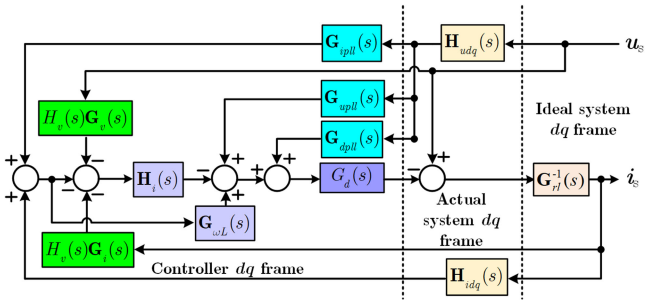

Fig. 8. Small-signal block diagram of the 4QC.

Due to the delay of the digital control and PWM [35], the relationship between the reference signal of the modulation voltage and the actual modulation voltage is expressed as

$$\begin{bmatrix}\Delta u_{abd}^{s}\\ \Delta u_{abq}^{s}\end{bmatrix} = G_d(s)\begin{bmatrix}\Delta u_{abdref}^{s}\\ \Delta u_{abqref}^{s}\end{bmatrix} \tag{16}$$

where $G_d(s) = e^{-T_d s}$ and T_d is the delay time of the PWM. According to the principle of Taylor series expansion, and neglecting the high-order items, in the low-frequency range, it will then be equivalent to a one-order inertial link

$$G_d(s) = \frac{1}{T_d s + 1}. \tag{17}$$

5) Impedance Model of One 4QC: In summary, the small-signal block of the 4QC is shown in Fig. 8.

The impedance-based model of the 4QC in the ideal system *dq-frame* can be expressed as

$$\begin{aligned}\mathbf{Z}_{dq} = &\left[\mathbf{I} - G_d\left[\left(\mathbf{G}_{dpll}+\mathbf{G}_{upll}\right)\mathbf{H}_{udq} + H_v\mathbf{H}_i\mathbf{G}_v\right.\right.\\ &\left.+\left(\mathbf{H}_i+\mathbf{G}_{\omega L}\right)\mathbf{G}_{ipll}\mathbf{H}_{udq}\right]\Big]^{-1}\\ &\cdot\left[\mathbf{G}_{rl} + H_v G_d \mathbf{H}_i\mathbf{G}_i + G_d\left(\mathbf{H}_i+\mathbf{G}_{\omega L}\right)\mathbf{H}_{idq}\right].\end{aligned} \tag{18}$$

The trains can be simplified as the paralleled result of 4QC with different numbers. Hence, the equivalent impedance of one train is defined as

$$\mathbf{Z}_{dq}^{t}(s) = \frac{1}{p}\mathbf{Z}_{dq}(s) \tag{19}$$

where p is the number of paralleled 4QCs.

Remark 3: An electric train is a typical single-phase ac system, owning a virtual but nonexistent β-axis, which differs from a balanced three-phase system. As a result, the single-phase system usually adopts some approaches, such as T/4 delay, or SOGI to transfer the α-axis. The T/4 delay can guarantee the orthogonal signal at the fundamental frequency, yet it could introduce phase angle errors at the other frequencies. Alternatively, the SOGI can obtain a 90° shifting at all frequencies, yet it also leads to an amplitude error at other frequencies. Therefore, the errors of amplitude and/or angle are inevitable, regardless of how we define or introduce the virtual β-axis for a single-phase system.

6) Analytical Negative Resistor of the Train Impedance: In (18), the terms affected by PLL can be extracted and expressed as

$$\begin{cases}\mathbf{A} = \left(\mathbf{G}_{dpll}+\mathbf{G}_{upll}\right)\mathbf{H}_{udq}\\ \mathbf{B} = \left(\mathbf{H}_i+\mathbf{G}_{\omega L}\right)\mathbf{G}_{ipll}\mathbf{H}_{udq}.\end{cases} \tag{20}$$

In (20), the voltage unit feedforward is considered. Moreover, for steady-state values, the relationship between the ac voltage and the modulation voltage of the rectifier can be expressed as

$$\begin{cases}u_{abdref}^{0} = u_d^0 + \omega_0 L i_q^0\\ u_{abqref}^{0} = -\omega_0 L i_d^0.\end{cases} \tag{21}$$

Due to the low-power operation mode of the rectifier, the approximate relationships $u_{abdref}^{0} \approx u_d^0, i_d^0 \approx 0$ can be obtained. Substituting them into (20), it can be found that the impact of PLL on the impedance is slight under the low-power operation mode with considering the voltage unit feedforward. Therefore, to simplify the impedance model, the PLL can be neglected in analyzing the LFO.

Furthermore, to clarify the impacts of the control loops on the impedance model, the simplified and analytical impedance model is derived in the controller *dq*-frame as [21]

$$\mathbf{Z}_{dq}^{c}(s) = \begin{bmatrix}Z_{dd}^{c}(s) & Z_{dq}^{c}(s)\\ Z_{qd}^{c}(s) & Z_{qq}^{c}(s)\end{bmatrix} \tag{22}$$

where

$$\begin{cases}Z_{dd}^{c}(s) = \frac{\Delta u_d^c}{\Delta i_d^c} = \frac{R+sL+G_d(s)H_i(s)+G_d(s)H_i(s)H_v(s)G_1(s)}{1-G_d(s)-G_d(s)H_i(s)H_v(s)G_3(s)}\\ Z_{dq}^{c}(s) = \frac{\Delta u_d^c}{\Delta i_q^c} = -\frac{[1-G_d(s)]\omega_0 L}{1-G_d(s)-G_d(s)H_i(s)H_v(s)G_3(s)}\\ Z_{qd}^{c}(s) = \frac{\Delta u_q^c}{\Delta i_d^c} = \omega_0 L\\ Z_{qq}^{c}(s) = \frac{\Delta u_q^c}{\Delta i_q^c} = \frac{R+sL+G_d(s)H_i(s)}{1-G_d(s)}.\end{cases}$$

In the low-power operation mode, the transfer function $G_3(s)$ can be neglected due to the small d-channel current. We let $s = j\omega$ and neglect the higher order items (the order of ω is more than two order). The detailed and analytical impedance is expressed as

$$\begin{cases}Z_{dd}^{c}(j\omega) \approx R + \frac{1}{T_d}\left(L - \frac{K_{iC}}{\omega^2} - \frac{0.5mK_{pC}K_{pV}}{\omega^2 C_d}\right)\\ \qquad\qquad +j\left(\omega L - \frac{R+K_{pC}}{T_d\omega}\right)\\ Z_{dq}^{c}(j\omega) \approx -\omega_0 L\\ Z_{qd}^{c}(j\omega) \approx \omega_0 L\\ Z_{qq}^{c}(j\omega) \approx R + \frac{1}{T_d}\left(L - \frac{K_{iC}}{\omega^2}\right) + j\left(\omega L - \frac{R+K_{pC}}{T_d\omega}\right)\end{cases} \tag{23}$$

where $m = u_d^0/u_{dc}^0$, u_d^0 is the steady d-channel voltage, and u_{dc}^0 is the steady dc-link voltage.

From (23), it can be found that the dc-link voltage PI controller will cause the negative resistor in the *d-d* channel impedance and the integral gain of CC will also cause the negative resistor in both the *d-d* channel impedance and *q-q* channel impedance. These will initiate the negative resistor area (NRA) of the train's impedance. The negative resistor can be expressed simply as

$$R_{ne}(j\omega) = -\frac{K_{iC}}{T_d\omega^2} - \frac{0.5mK_{pC}K_{pV}}{T_d C_d \omega^2}. \tag{24}$$

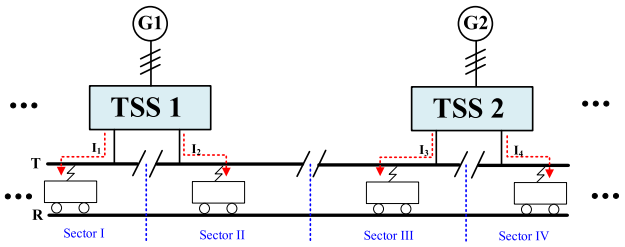

Fig. 9. Power supply sectors in the electric railway.

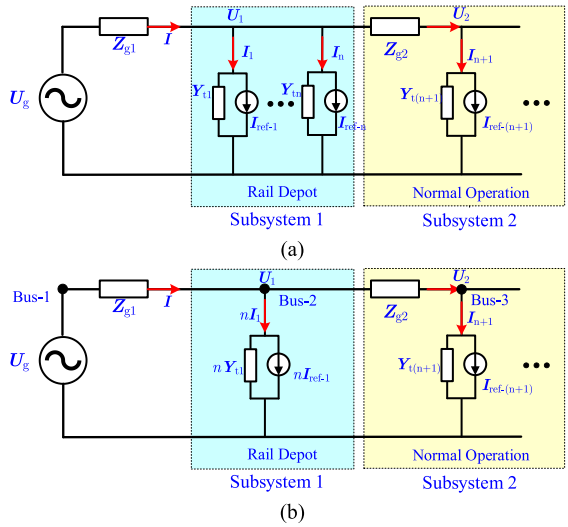

Fig. 10. Multitrain interaction system in one power supply sector. (a) Circuit model. (b) Simplified model.

In (24), due to $0.5m/C_d \gg 1$, the impact of the dc-link voltage PI controller on the negative resistor is more sensitive than that of the integral gain of CC. The impact of negative resistor on the LFO in the train-network system will be carefully discussed in the following section.

IV. Mechanism and Influential Factors of LFO

In the conventional ac electric railway, every power supply sector, shown in Fig. 9, is separated. The LFO easily occurs when multiple trains are simultaneously energized in a rail depot. Hence, this article focuses only on one power supply sector.

The multitrain interaction system in one power supply sector can be equivalent to the circuit model shown in Fig. 10(a), which includes energized trains in the rail depot, normal operation trains, and impedance of the traction network system. It should be noted that the energized trains in the rail depot have the same operation condition and their energized points are close to each other. Therefore, the energized trains in the rail depot can be aggregated as one impedance, as shown in Fig. 10(b).

Furthermore, in Fig. 10(b), the multitrain interaction system considers different operation conditions and different energized positions of trains. Taking the 3-bus system shown in Fig. 10(b) as an example, according to the impedance aggregation theory [48], [49], at Bus-2, the equivalent impedance of the load modulus can be aggregated as follows:

$$\mathbf{Y}_L(s) = n\left[\mathbf{Z}^t_{dq}(s)\right]^{-1} + \left[\mathbf{Z}^g_{dq-2}(s) + \mathbf{Z}^t_{dq-(n+1)}(s)\right]^{-1} \tag{25}$$

where n is the number of energized trains in a rail depot.

Therefore, the multitrain interaction system can also be analyzed by the impedance-ratio criterion. Additionally, in (25), it can be found that the paralleled normal operation train will reduce the magnitude of the equivalent load impedance, which implies that the accepted number of the energized trains in the rail depot will be reduced. Moreover, the stability of the subsystem 2 in Fig. 10(b) should be also checked to avoid the local instability before impedance aggregation. In this article, we focus on the mechanism analysis of the LFO to enable the number of normal operating trains in (25) is taken as zero. Therefore, the impedance-ratio matrix of the train-network system is derived as

$$\mathbf{T}_{dq}(s) = n\mathbf{Z}^g_{dq}(s) \times \left[\mathbf{Z}^t_{dq}(s)\right]^{-1}. \tag{26}$$

A. Formation Mechanism of the LFO

In the dq-frame, the impedance ratio matrix of the train-network system in (26) is one 2×2 matrix. For this multiple input and multiple output (MIMO) system, the stability can be determined by the generalized Nyquist criterion (GNC) [50]. If the Nyquist curves of the eigenvalues of (26) encircle the point (–1, 0) in the s plane, the train-network system is unstable. To calculate the eigenvalues, the impedance ratio matrix can be transformed from the dq domain to the modified sequence domain [51], [52]. The impedance-ratio matrix in the modified sequence domain is expressed as

$$\mathbf{T}_{seq}(s) = \boldsymbol{A}_Z \cdot \mathbf{T}_{dq}(s) \cdot \boldsymbol{A}_Z^{-1} \tag{27}$$

where $\boldsymbol{A}_Z = \frac{1}{\sqrt{2}}\begin{bmatrix} 1 & j \\ 1 & -j \end{bmatrix}$, $\boldsymbol{A}_Z^{-1} = \boldsymbol{A}_Z^{\mathrm{H}} = \frac{1}{\sqrt{2}}\begin{bmatrix} 1 & 1 \\ -j & j \end{bmatrix}$.

Furthermore, (27) can be expanded as

$$\begin{aligned}\mathbf{T}_{seq}(s) &= n \cdot \boldsymbol{A}_Z \cdot \mathbf{Z}^g_{dq}(s) \cdot \boldsymbol{A}_Z^{-1} \cdot \left[\boldsymbol{A}_Z \cdot \mathbf{Z}^t_{dq}(s) \cdot \boldsymbol{A}_Z^{-1}\right]^{-1} \\ &= n \begin{bmatrix} Z^g_{pp}(s) & 0 \\ 0 & Z^g_{nn}(s) \end{bmatrix} \begin{bmatrix} Y^t_{pp}(s) & Y^t_{pn}(s) \\ Y^t_{np}(s) & Y^t_{nn}(s) \end{bmatrix}.\end{aligned} \tag{28}$$

It should be noted that the transformation from the dq domain to the modified sequence domain is linear, and the eigenvalues of the impedance ratio matrixes of (26) and (28) are the same [51]. The accurate eigenvalues can be expressed as

$$\lambda_{1,2} = n\frac{\left(Z^g_{pp}Y^t_{pp} + Z^g_{nn}Y^t_{nn}\right) \pm \sqrt{\left(Z^g_{pp}Y^t_{pp} - Z^g_{nn}Y^t_{nn}\right)^2 - Z^g_{pp}Z^g_{nn}Y^t_{pn}Y^t_{np}}}{2}. \tag{29}$$

In the modified sequence domain, the network's impedance is a diagonal matrix due to its symmetry. In addition, due to the asymmetry of controller, the train's impedance is a nondiagonal but diagonally dominant matrix. Then, neglecting the nondiagonal elements of train's impedance matrix in the modified

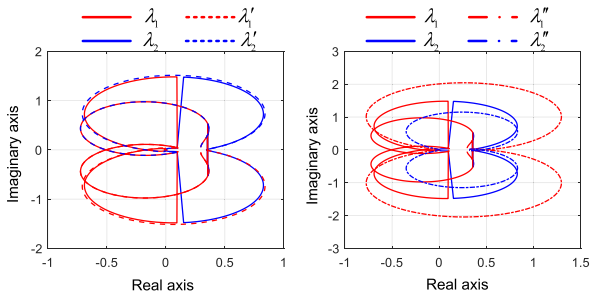

Fig. 11. Comparisons of eigenvalues in different domains. (a) Comparison between approximate eigenvalues in the modified sequence domain and accurate eigenvalues in the *dq* domain. (b) Comparison between approximate eigenvalues in the *dq* domain and accurate eigenvalues in the *dq* domain.

sequence domain, the approximate eigenvalues are defined as

$$\begin{cases} \lambda'_1(s) \approx nZ^g_{pp}(s)Y^t_{pp}(s) = n\frac{Z^g_{pp}(s)}{Z^t_{pp}(s)} \\ \lambda'_2(s) \approx nZ^g_{nn}(s)Y^t_{nn}(s) = n\frac{Z^g_{nn}(s)}{Z^t_{nn}(s)}. \end{cases} \tag{30}$$

The comparison between the approximate eigenvalues in the modified sequence domain and the accurate eigenvalues in the *dq* domain is shown in Fig. 11(a), which indicates that the nondiagonal elements of the train's impedance matrix in the modified sequence domain have a slight impact.

Similarly, in the *dq*-domain, both the train's impedance matrix and the network's impedance are not diagonally dominant matrices. The reason is that the coupling terms $\omega_0 L$ and $\omega_0 L_s$ have an obvious impact on the eigenvalues in the low-frequency range. Some references neglect the off-diagonal elements in *dq*-domain [53], and then, the approximate eigenvalues are defined as

$$\begin{cases} \lambda''_1(s) \approx nZ^g_{dd}(s)Y^t_{dd}(s) = n\frac{Z^g_{dd}(s)}{Z^t_{dd}(s)} \\ \lambda''_2(s) \approx nZ^g_{qq}(s)Y^t_{qq}(s) = n\frac{Z^g_{qq}(s)}{Z^t_{qq}(s)}. \end{cases} \tag{31}$$

The comparison between the approximate eigenvalues and the accurate eigenvalues in the *dq*-domain is shown in Fig. 11(b), which indicates that the coupling terms $\omega_0 L$ and $\omega_0 L_s$ have obvious impact on the eigenvalues in the *dq*-domain. Therefore, the approximation is not suitable for analyzing the LFO.

In summary, in the modified-sequence domain, the system can be approximately decoupled as two single input and single output (SISO) systems, which is convenient for revealing the impedance interaction mechanism and maintains the accuracy. It should also be noted that although the impacts of the nondiagonal elements on the stability analysis in the modified sequence domain are slight, neglecting the nondiagonal elements of the impedance ratio matrix in modified sequence domain could cause an optimistic stability analysis result in some critical cases [54].

To obtain the magnitude and phase information of eigenvalues, let $s = j\omega$, and the eigenvalues in (30) are rewritten as

$$\begin{cases} \lambda'_1(j\omega) \approx n\frac{|Z^g_{pp}(j\omega)|}{|Z^t_{pp}(j\omega)|}\left[\angle Z^g_{pp}(j\omega) - \angle Z^t_{pp}(j\omega)\right] \\ \lambda'_2(j\omega) \approx n\frac{|Z^g_{nn}(j\omega)|}{|Z^t_{nn}(j\omega)|}\left[\angle Z^g_{nn}(j\omega) - \angle Z^t_{nn}(j\omega)\right]. \end{cases} \tag{32}$$

The interactive stability of the train-network system can be analyzed by plotting the frequency response of (32). If the phase margins (PM) of all eigenvalues are positive, then the system is stable [55], which conforms to

$$\begin{cases} -180^\circ < \angle Z^g_{pp}(j2\pi f_{m1}) - \angle Z^t_{pp}(j2\pi f_{m1}) < 180^\circ \\ -180^\circ < \angle Z^g_{nn}(j2\pi f_{m2}) - \angle Z^t_{nn}(j2\pi f_{m2}) < 180^\circ \end{cases} \tag{33}$$

where f_{m1} and f_{m2} are magnitude crossover frequencies of the eigenvalues.

If the train-network system is a minimum phase system and the impact of the off-diagonal elements in the train-impedance matrix are neglected. Therefore, it is important to note that (33) is a necessary and sufficient condition for a stable system.

It is known that the impedance of the network is passive and its phase characteristic is always in the range –90° to +90° [56]. The negative resistor introduced in (24) will cause the phase characteristic of Z^t_{pp} and Z^t_{nn} to be out of the ±90° region, which could cause the phases of the eigenvalues to be out of the ±180° region in some frequency ranges. This frequency range is defined as the unstable frequency range of the eigenvalues. With increasing numbers of energized trains in a rail depot or a weak traction network, the magnitude crossover frequency could move into unstable frequency range, which would then lead to a negative PM of the train-network system, thus exciting an LFO.

According to (32), the stability of the train-network system depends on whether the PM at the magnitude crossover frequency is outside the limits of ±180° or not. In particular, the frequency range of 1–10 Hz is mainly considered for the LFO. The magnitudes of the eigenvalues are independently expressed as

$$M_1(j\omega) = n\frac{\left|Z^g_{pp}(j\omega)\right|}{\left|Z^t_{pp}(j\omega)\right|}, M_2(j\omega) = n\frac{|Z^g_{nn}(j\omega)|}{|Z^t_{nn}(j\omega)|}. \tag{34}$$

Therefore, if both M_1 and M_2 are smaller than 0 dB in 1–10Hz, there will be no magnitude crossover frequencies in 1–10Hz and the system will be stable. In other words, both reducing the magnitude of the network impedance and increasing the magnitude of the train impedance in the low-frequency range are beneficial to stabilize the system.

Moreover, the phases of all eigenvalues are also independently expressed as

$$\begin{cases} \varphi_1(j\omega) = \arctan\left[\frac{\mathrm{Im}(Z^g_{pp}(j\omega))}{\mathrm{Re}(Z^g_{pp}(j\omega))}\right] - \arctan\left[\frac{\mathrm{Im}(Z^t_{pp}(j\omega))}{\mathrm{Re}(Z^t_{pp}(j\omega))}\right] \\ \varphi_2(j\omega) = \arctan\left[\frac{\mathrm{Im}(Z^g_{nn}(j\omega))}{\mathrm{Re}(Z^g_{nn}(j\omega))}\right] - \arctan\left[\frac{\mathrm{Im}(Z^t_{nn}(j\omega))}{\mathrm{Re}(Z^t_{nn}(j\omega))}\right]. \end{cases} \tag{35}$$

In (35), it is interesting to see that when the total impedance of the traction network is constant, the larger resistance part of network impedance leads to a more stable system. In contrast, the negative resistance of the electric train, using the same assumption, and its range should be smaller in order to stabilize the system. The impact of the resistance to the overall impedance is also important in the LFO analysis.

Remark 4: The above analysis comprehensively investigated the condition of the instability in the low-frequency region. It relates to the equivalent impedance (including the number

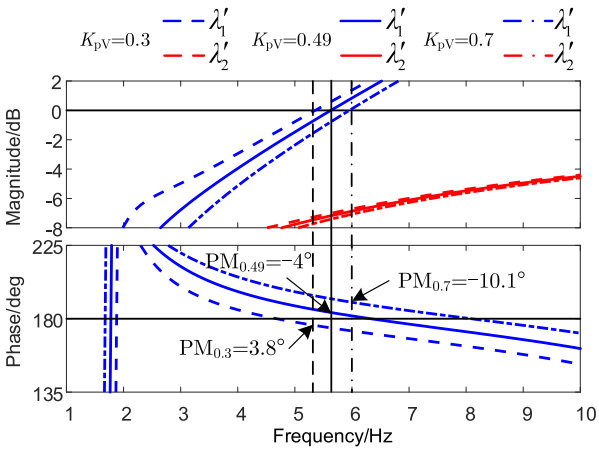

Fig. 12. Frequency responses of the eigenvalues under different K_{pV}.

of trains), X / R (including the angle difference between the network and converter), and the negative resistance of the train (corresponding to the controller dynamics of trains). Moreover, these factors explain the phenomena and characteristics of the field measured waveforms.

B. Impact of the Electric Train

According to (32), it is a good choice to reduce the unstable frequency range and the magnitudes of the eigenvalues to enhance the stability of the train-network system. In other words, for the train-impedance, reducing its NRA and increasing its magnitude are beneficial for suppressing the LFO. To investigate the factors that influence the initiation of LFO in the interaction between the traction network and the electric trains, a numerical model for each part of this system has been reported in studies.

1) Impact of the DC-Link Voltage Controller: By (24), K_{pV} has a significant influence on the real part of the train impedance. Increasing K_{pV} will expand the NRA and slightly increase the magnitude [21]. Therefore, K_{pV} can be regarded as only affecting the phase difference at the same crossover magnitude frequency when the network impedance is fixed. In addition, increasing K_{pV} means that the bandwidth of the dc-link voltage controller is increased [57]. Therefore, a wider bandwidth of the dc-link voltage controller leads to a good dynamic response of the dc-link voltage, on the other hand, it results in higher potential of instability to the train-network system.

In Fig. 12, with K_{pV} decreasing, the crossover magnitude frequency of the eigenvalue changes just a little, while the NRA region is significantly narrowed, which gradually reduces the phase at the crossover magnitude frequency to less than 180°. Therefore, decreasing the bandwidth of the dc-link voltage controller helps to stabilize the system.

2) Impact of the Current Controller: The analytic expression in (24) also indicates that K_{pC} dominates both the real and imaginary parts of the train impedance. Therefore, this factor has a significant influence on both the NRA and the magnitude of train impedance at the same time [21]. The stability of the train-network depends on the magnitude crossover frequency

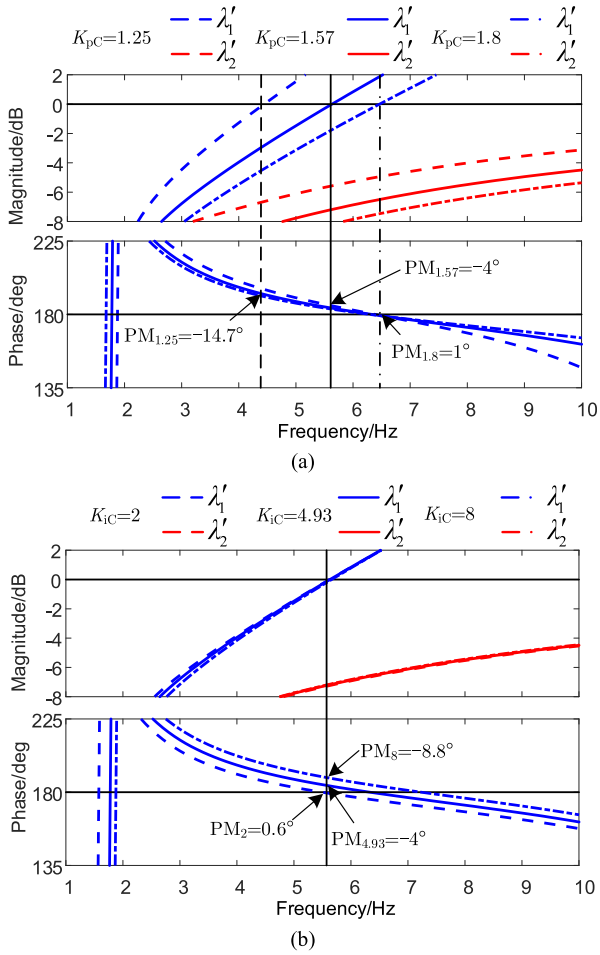

Fig. 13. Frequency responses of the eigenvalues: (a) under different K_{pC}; (b) under different K_{iC}.

being located in the unstable frequency range or not after changing K_{pC}. In Fig. 13(a), increasing K_{pC} causes the crossover frequency to move out of the unstable frequency range. In addition, in (24), the integral gain also causes negative resistance. As seen in Fig. 13(b), increasing K_{iC} will expand the unstable frequency range of the eigenvalues and has a slight impact on the magnitude.

3) Impact of the Circuit Parameters: As shown in (24), enhancing the dc-link capacitor C_d decreases the NRA of the input converters, nonetheless, the imaginary part of the train impedance is less impacted. As a result, increasing C_d reduces the phase difference without changing the crossover magnitude frequency of the eigenvalue, and it stabilizes the system by means of the stability margin improvement. In Fig. 14, three different C_d are simulated, the phase margin is changed from negative to positive, which implies that a larger C_d has a positive impact on suppressing LFO.

On the other hand, as shown in Fig. 15, increasing the resistor of the onboard transformer not only reduces the NRA by providing a positive resistance, but also increases the crossover magnitude frequency, which can, additionally, stabilize the LFO.

From (24), the inductance L of the onboard transformer has a significant impact on both the real and imaginary parts of the

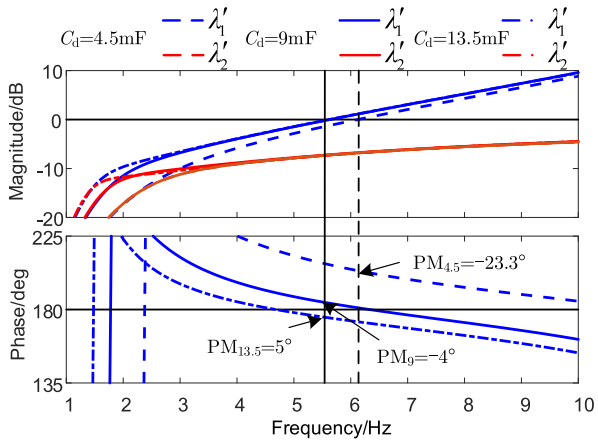

Fig. 14. Frequency responses of the eigenvalues under different values of C_d.

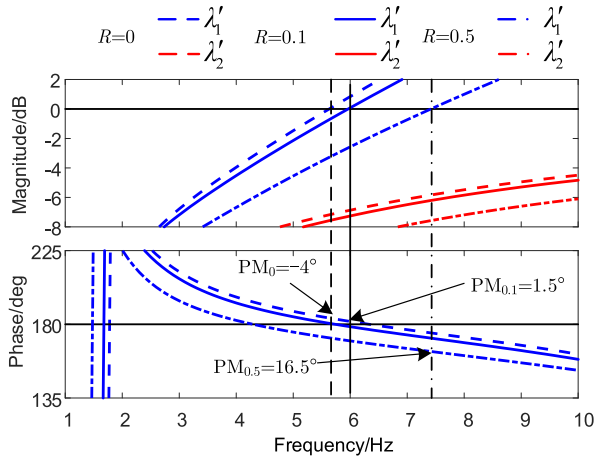

Fig. 15. Frequency responses of the eigenvalues under different values of *R*.

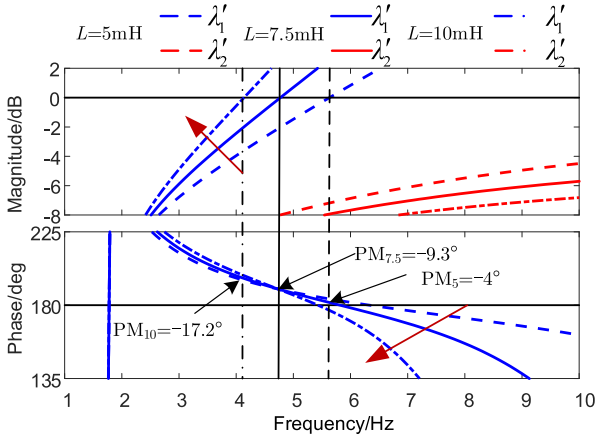

Fig. 16. Frequency responses of the eigenvalues under different values of *L*.

train impedance, which means that its influence on the LFO also depends on the magnitude crossover frequency being located in the unstable frequency range or not after changing the *L*. In Fig. 16, although increasing the inductance *L* of the onboard transformer narrows the unstable frequency range, the crossover

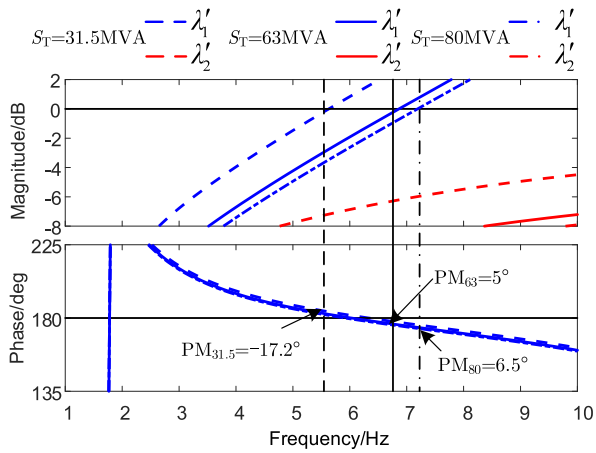

Fig. 17. Frequency responses of the eigenvalues to different values of S_T.

magnitude frequency will approach zero more quickly as *L* increases, and fall back into the unstable frequency range.

4) Impact of the Total Traction Network Impedance: According to the model of the traction network earlier presented, the impedance on the traction side mainly consists of the power grid, traction transformer, and catenary line.

In a traditional power system, the short-circuit ratio (SCR) is an indication of the system strength [58]. A more stable systems is equipped with a larger SCR. As a corollary to this concept in traction power systems, the SCR can also characterize the stability of the train-network system as

$$\mathrm{SCR}_t = \frac{S_{\mathrm{Network}}}{S_{\mathrm{Train}}} = \frac{U_B^2}{Z_g} \Big/ (nP_{\mathrm{Train}}). \tag{36}$$

In (36), S_{Network} is the equivalent capacity of the traction network, S_{Train} represents the total rated capacity of the energized electric trains, U_B is the secondary voltage of the traction transformer, *n* represents the number of trains, and P_{Train} represents the rated power of a single train. When the rated power of the trains is fixed, SCR_t is related to the impedances of both the traction network and the number of trains. Increasing Z_g and *n* will reduce SCR_t, implying that the system is more prone to instability.

As earlier shown in the previous analysis, the traction transformer and catenary line impedances dominate the overall impedance of the traction network. Increasing the capacity of the traction transformer will decrease the impedance of the traction network, while the impedance of the traction network in 1 × 25 kV network is also greater than that in the AT network. Therefore, the eigenvalue frequency responses under different S_T or different power supply modes are obtained as shown in Figs. 17 and 18. With S_T increasing, the phase response stays nearly the same, while the magnitude declines significantly. Therefore, crossover frequency falls outside the unstable frequency range. Similarly, although the phase characteristics of ATs are slightly higher than the other two, magnitude characteristic of eigenvalues under ATs is the smallest. Thus, the phase margin is still reduced.

TABLE V
MAIN PARAMETERS OF THE TRAIN-NETWORK SYSTEM AND THEIR INFLUENCE ON THE SYSTEM'S IMPEDANCE AND STABILITY

	Parameters	Network resistance	Network impedance	Train negative resistance	Train impedance	Stability
Network	Utility capacity	−	−	None	None	+
	Capacity of traction transformer	− − −	− − −			+ + +
	U_k% of traction transformer	None	+ + +			− − −
	Catenary length	+ +	+ +			− −
Trains	Proportional gain of DVC K_{pV}	None	None	+ + +	+	− − −
	Integral gain of DVC K_{iV}			+	+	−
	Proportional gain of CC K_{pC}			+ + +	+ + +	Undefined
	Integral gain of CC K_{iC}			+ +	+	− −
	DC-link C_d			− − −	−	+ + +
	Onboard transformer L			− −	− −	Undefined
	Onboard transformer R			− − −	+ + +	+ + +
	Quantity			None	− − −	− − −

Notes: "+" represents a positive influence on the indices and "−" represents a negative influence on the indices.

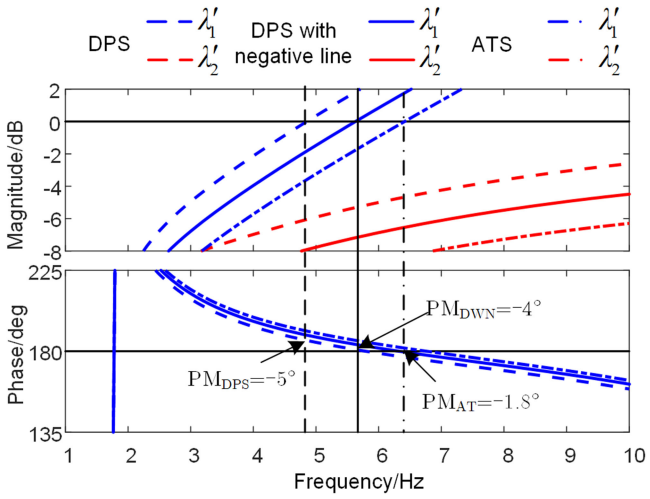

Fig. 18. Frequency responses of the eigenvalues under different supply modes.

5) Summary and Comments: The above analyses of the train-network interaction system under diverse conditions depict that the changes in the source and load subsystem parameters have a significant impact on the LFO of the interaction system. The main factors considered in the source subsystem are the catenary length, short-circuit capacities of regional power grid, and the capacity of traction transformer. The primary factors for the load subsystem include the number, electrical parameters, and control parameters of trains. Therefore, it can be concluded that such changes of the main factors affect the stability of interaction systems through changes to the system's impedance. Moreover, the LFO gives a measure of the system stability. These factors and their effects are summarized in Table V, where only one factor is changed at a time.

In addition, based on the previous discussion, the sensitivity of factors is also qualitatively depicted in Table V. In the traction network, the traction transformer in substation plays an important part of the network impedance. Therefore, the capacitor and U_k% of traction transformer in substation should be carefully designed to avoid a weak traction network. For the parameters

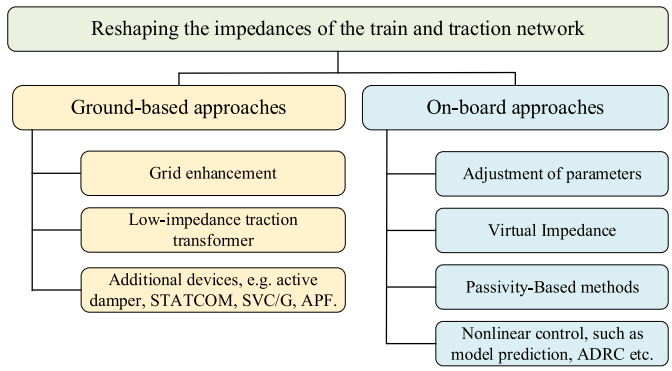

Fig. 19. LFO elimination methods.

of the train, apart from the train quantities, K_{pV}, K_{pC}, C_d, and R are the main influential factors on the train impedance. However, it should be noted that the impact of changing K_{pC} and L on the system stability remains undefined. The smaller the bandwidth of the dc-link voltage controller, the larger the dc-link capacitor, and the addition of appropriate resistance to the onboard transformer is beneficial to avoiding the LFO.

V. LFO MITIGATION APPROACHES

A. Overview of the Available LFO Elimination Approaches

As the LFO phenomenon is induced on both the traction network and the electric train, it is possible to mitigate the LFO via ground-based and on-board approaches. The existing methodologies are classified in Fig. 19. The underlying principle of these suppression methods is to reshape the impedance of the train-network system.

On the network side, Wang *et al.* [8] proposed either voltage stabilizers installed in the substations or a upgraded capacity of the traction transformer. Liu *et al.* [59] and Wu *et al.* [60] proposed the addition of an active compensator to a substation. On the other hand, for the train part of the system, the influence of train number and the controller parameters are the main considerations. Reducing the number of trains connected to the

TABLE VI
SYSTEM PARAMETERS IN XUZHOU TSS

Parameters		Before Changes	After Changes
Utility Grid	U_g/kV	110	110
	S_{SC}/MVA	938	938
Traction Transformer	S_T/MVA	31.5	50
	U_k%	10.5	8.4
Catenary Network	$r_i\angle\varphi_i$	0.32∠73°	0.32∠73°
	l/km	7	7
SCR$_t$		1.69(n=6)	2.50(n=6)

catenary can decrease the severity of LFO, but it results in the loss of capacity and flexibility of the transport system. Thus, this method can only be applied only as a temporary emergency intervention. Alternative techniques can be divided into four categories, which are the adjustment of the controller parameters [61], virtual-impedance-based methods [21], passivity-based methods [62], and new nonlinear control strategies [63].

Because all of the aforementioned propositions require substantial investments and alterations in the existing traction system infrastructure. In addition, demanding efforts are required for the controller design of the train-network system. As a result, effective and less invasive methods for mitigating LFO are yet to be realized. Therefore, further investigations are still needed to achieve effective LFO mitigation with the minimal modifications to the existing train-network system.

B. Mitigation Cases in Ground-Based Approaches

1) Grid Enhancement: It can be concluded that the impedance of a traction transformer is the dominant parameter on the traction network side. Therefore, reducing the short-circuit voltage ratio and increasing the capacity of the transformer are effective in decreasing its impedance. For instance, the case of addressing LFO problems in the Xuzhou TSS, effective results have been achieved by increasing the capacity of the transformer from 31.5 to 50 MVA and reducing the short-circuit voltage percentage of the transformer from 10.5% to 8.4%. The main parameters of the Xuzhou TSS are shown in Table VI. Before the transformer capacity was increased, the maximum number of the accepted energized trains was approximately 6. Under this condition, the SCR$_t$ of the Xuzhou TSS was approximately 1.69. For further clarity, consider the case of keeping the energized train number fixed, after changing the transformer, the SCR$_t$ increases to 2.5, which indicates that the accepted train number is almost doubled.

After the updated transformer was commissioned, field tests indicated that the traction network was enhanced to support the simultaneous energizing of 13 trains at the rail depot. These results are illustrated in Fig. 20.

2) Installation of Additional Devices: According to the measured waveforms of the LFO, it is seen that the active and reactive powers fluctuate periodically. Therefore, some research works introduced the static synchronous compensator (STATCOM) to dynamically compensate the reactive power of the train-network system [59]. In fact, the STATCOM, similar to an active damper [64], modifies the effective impedance of the traction network system. Similarly, the active power filter (APF) can be also

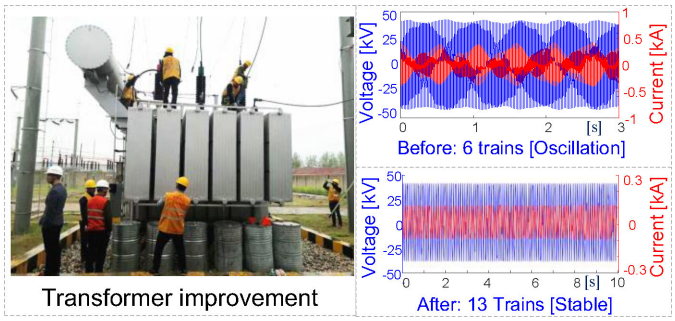

Fig. 20. Grid enhancement for eliminating LFO.

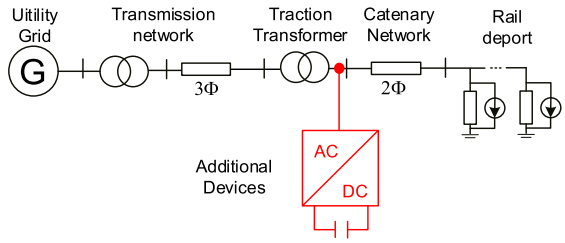

Fig. 21. Additional devices for eliminating LFO.

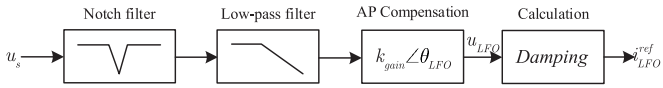

Fig. 22. Additional damping controller for suppressing the LFO.

used to change the impedance of the traction network and compensate the harmonics [60]. These additional devices are usually connected to the traction station as shown in Fig. 21.

Alternatively, some additional damping control schemes are introduced to regulate the operation of these compensating devices in order to provide controlled damping [65], [66]. The additional damping controller typically includes the detection and calculation of the compensation current. Fig. 22 shows a basic scheme to extract the low-frequency component and calculate the compensation current for the provision of enhanced damping characteristics in the train-network system [67].

These compensators achieve dynamic compensation by detecting the real-time variations to voltage and current references. Therefore, they have no impact when system works under normal, steady-state conditions. Nonetheless, their complicated structure and high cost limit their practical applications. Additionally, the design of their controller for the suppression LFO introduce further instability problems.

C. Mitigation Approaches in On-Board Controllers

1) Optimization of the Parameters of the Controllers: As discussed in the previous section, tuning of the controller parameters can enhance the dynamic performance and stability of the interaction system for multiple trains in a light-loading working condition. This contributes to realizing the matching relation between the controller and the controlled plant. This result can then be further extended for effective and economic

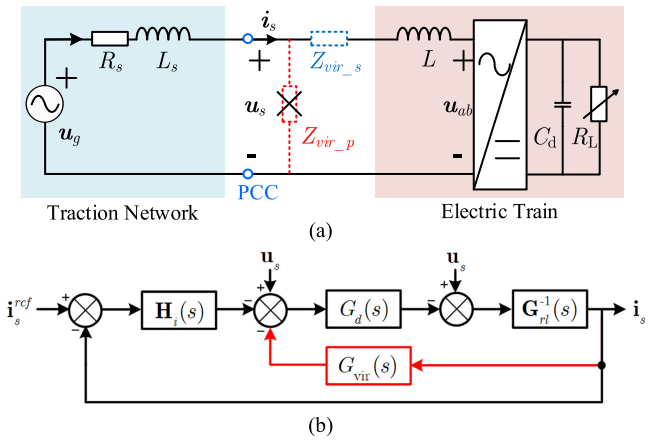

Fig. 23. (a) Schematic diagram of series virtual impedance. (b) Block diagram of the current feedback [21].

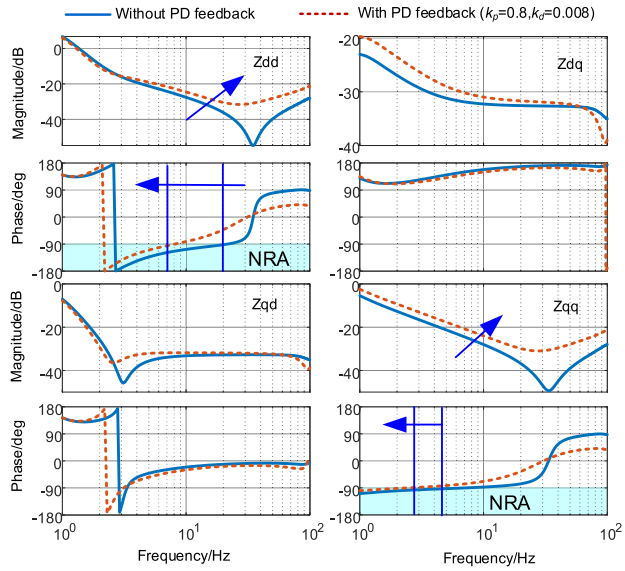

Fig. 24. Train impedance with/without P-D feedback of current.

suppression, providing the effect of mitigating the LFO in an ac electrified railway. The detailed influence laws are summarized in Table VI, which provides a useful reference for tuning of parameters in engineering applications. In summary, parameters optimization is an easy and low-cost suppression method for LFO. However, the requirements for good dynamic performance of electric trains limit the selected range of these parameters.

2) Virtual-Impedance-Based Suppression: In Fig. 15, when the input resistance increases, the oscillation frequency shifts to the right-half plane and the unstable frequency range reduces accordingly to enhance the system stability. However, increasing the input resistance also results in higher power losses.

To enhance the controllability for reshaping the impedance of the converter and to reduce the power loss of the real impedance, the virtual impedance-based suppression method was developed. The virtual impedance can provide the expected impedance of the train in any frequency range by designing a feedback loop or feed-forward loop [68]. In addition, it avoids an actual power loss and gives a physical insight into the different feedback/feed-forward control loops [69]. In general, series and parallel virtual impedances are the two main methods, as shown in Fig. 23(a). However, as mentioned in the previous section, higher magnitude and narrower range of the NRA are expected. So, a series virtual impedance in the form of $R_{\rm vir} + jX_{\rm vir}$ (where $R_{\rm vir} > 0$ and $X_{\rm vir} > 0$) for the train impedance is suitable for suppressing the LFO.

Different feedback functions can achieve the desired compensation effects. A positive resistance in the low-frequency range is to compensate the negative resistance, and a positive reactance is initiated to increase the magnitude in low-frequency range. Zhou *et al.* [21] proposed a proportional-differential (P-D) feedback function of the current that is presented

$$G_{\rm vir}(s) = G_{\rm vir\_}{}_D(s) + G_{\rm vir\_}{}_P(s) \tag{37}$$

where $G_{\rm vir\_}{}_D(s) = -k_d \cdot s \cdot \frac{\omega_c}{s+\omega_c}$,$G_{\rm vir\_}{}_{\rm P}(s) = -k_p$.

From Fig. 23 and Fig. 24, the P-D feedback function of the current achieves a narrower NRA and a larger impedance of the train in the low-frequency range. However, the additional feedback or forward back loop will change the original structure of the controller, which may influence the dynamic performance of the converter. Therefore, the balance between the system stability and system dynamic performance still requires significant consideration. This informs the process of the parameter tuning and the self-adaption of the virtual-impedance-based control.

3) Passivity-Based Suppression Methods: Suppose that the electric train has a passive impedance behavior; the train-network system is guaranteed to be stable regardless of the number of trains, because the traction network consists of passive components [56], [70]. The energy function of the train can be expressed by the input voltage and input current as [32]

$$W = \frac{1}{2\pi}\int_{-\infty}^{\infty} {\rm Re}\left[u_d i_d^* + u_q i_q^*\right] d\omega \tag{38}$$

where ${\rm Re}[u_d i_d^* + u_q i_q^*] = \frac{1}{2}\mathbf{I}^{\rm H}\underbrace{[\mathbf{Z}_{dq}^c + (\mathbf{Z}_{dq}^c)^{\rm H}]}_{\mathbf{H}}\mathbf{I}$.

Based on the *dq* impedance in (23), matrix $\mathbf{H}$ is expressed as

$$\mathbf{H} = \begin{bmatrix} 2{\rm Re}(Z_{dd}^c) & (Z_{dq}^c + Z_{qd}^{c*})^* \\ Z_{dq}^c + Z_{qd}^{c*} & 2{\rm Re}(Z_{qq}^c) \end{bmatrix} \approx \begin{bmatrix} 2{\rm Re}(Z_{dd}^c) & 0 \\ 0 & 2{\rm Re}(Z_{qq}^c) \end{bmatrix}. \tag{39}$$

To keep the passivity behavior of the electric train, the matrix $\mathbf{H}$ should be a positive definite matrix [71], which means that the eigenvalues of (39) are always larger than zero in all frequency ranges.

However, due to the negative resistance behavior, (39) will not hold in the low-frequency range. Apart from passivity control based on the nonliner theory, Hu *et al.* [62] proposed utilizing the diode-bridge rectification mode to change the impedance of the 4QC in real time. Fig. 25 shows that the DBR mode is analogous to the normal mode in circuit structure. From Fig. 26(a), the equivalent impedance of the train in DBR mode is passive. Combating the real-time detection approaches of the LFO proposed in the previous section, as seen in Fig. 26(b), this method can effectively suppress voltage fluctuations of the

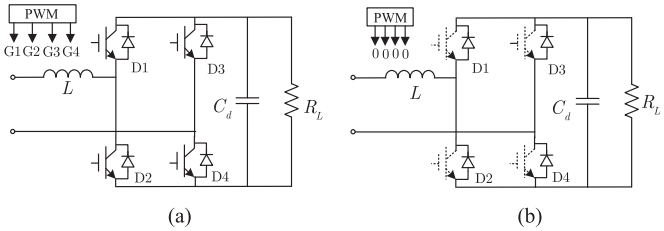

Fig. 25. Circuit structure of the two modes of the traction network. (a) Normal mode. (b) DBR mode.

TABLE VII
COMPARISON OF TECHNOLOGIES FOR SUPPRESSING LFO

Method	Cost	Performance	Real-time
Low impedance transformer in traction substation	High	Good	No
Compensator placement	High	Moderate	Yes
Control optimization	Low	Moderate	No
Operation mode adjustment	Moderate	Good	Yes
Virtual-impedance	Low	Moderate	No
Nonlinear controller	Low	Good	No

traction network, while it avoids traction atresia and protection malfunction.

4) Nonlinear Control: As discussed in the previous sections, the LFO is mainly caused by the dc-link voltage PI controller. Therefore, in order to avoid the disadvantages associated with linear controllers, some nonlinear controllers have been investigated for application to the train. These include autodisturbance rejection control (ADRC) [63], model predictive control [72] and interconnection, and damping assignment passivity-based control (IDA-PBC) [73]. These advanced control methods eliminate the impact of the dc-link voltage PI controller and enhance the robustness of the train. However, due to the complexity of these nonlinear controllers, their industrial applications are still largely limited.

D. Summary and Comments

The aforediscussed elimination approaches and their performances can be summarized in Table VII. Both the low-impedance transformers in the TSS and compensating devices, such as STATCOM, APF, have a high cost requirement. For example, the cost of increasing the capacity from 31.5 to 50 MVA is about 8 million RMB (USD 1.13 million). The low-impedance transformer has excellent suppression effect and does not introduce extraneous instability challenges. These devices can achieve dynamic compensation by detecting variations in the real-time voltages and currents.

On the other hand, the cost of control parameters optimization is relatively low and attractive to industry. For instance, in 2013 and 2014, the Shanghai Railway Bureau organized technicians of Alstom to adjust the control parameters to suppress the LFO. Nonetheless, due to the constraints on the range of parameter variation, this approach has unsatisfactory mitigation results. Thus, to maximize the equivalent impedance of the electric

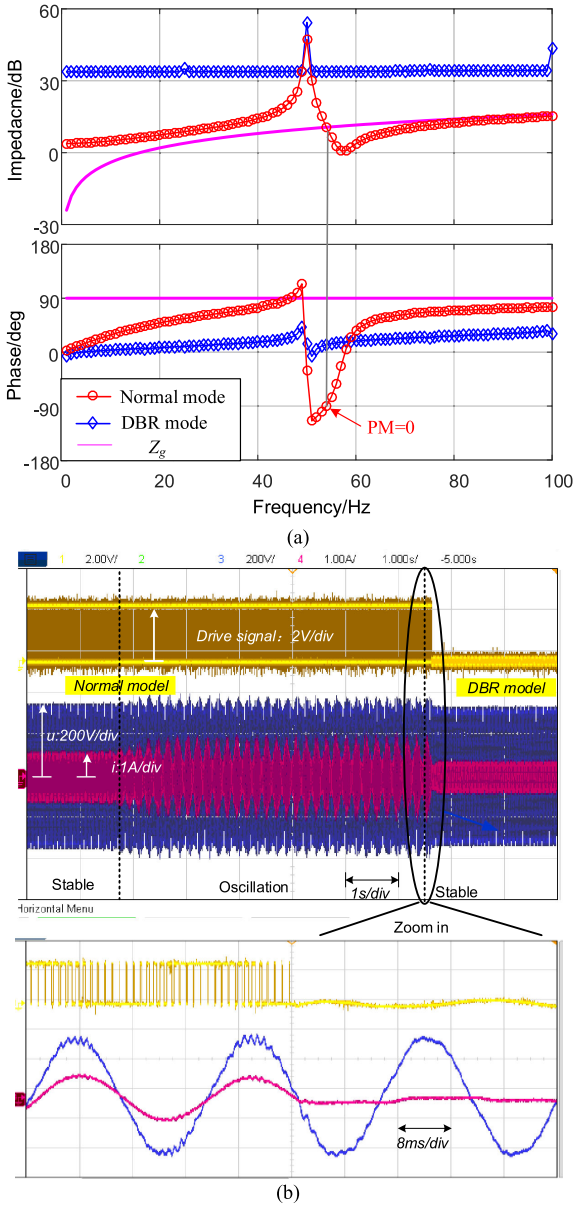

Fig. 26. Passivity-based method for eliminating the LFO. (a) Input impedance of the train under different mode. (b) Waveforms of changing operation mode of the train when the LFO arises [62].

train, the operation mode adjustment based on passivity theory is presently used by the Shanghai Railway Bureau.

Both the virtual impedance-based method and the nonlinear controllers aim to modify the structure of the train controller. The control parameters are fixed in the train's controller. When LFO occurs, the parameters cannot by easily modified in real time. Therefore, these methods can be combined with self-adaption methods to achieve the suppression of LFOs in real time [61].

VI. STANDARDS, DISCUSSION, AND RECOMMENDATIONS

A. Standards

The standard EN50388-2012 [74], which added new requirements from its previous version in 2005. For instance, it

described and classified the root causes of overvoltage events in the ac or dc electrified railways for oscillation (or instability) and harmonic problems. In EN50388-2012, the ac line voltage and current show an amplitude and phase modulation. The typical modulation frequency is from 10%–30% of the fundamental frequency. It is caused by the interaction between a four-quadrant converter train and the supply systems. The standard limits the voltage for ac 25 kV@50 Hz at a voltage range of 23–31 kV.

It is required to characterize or limit the input impedance of the train. For the high-frequency harmonic instability, it requires the fifth harmonic of the input impedance passively [75]. The low-frequency instability problem in EN50388-2012 for 4QC, the active and/or passive *RLC* are dependent on frequency and control. But for the remaining types of electric trains (diode rectifier, thyristor rectifier, and so on), passive RL is required when the frequency exceeds the fundamental frequency.

As seen from (24), the passivity of the train at all frequencies is impossible when the control structure and control method is not changed. The reason is in the *dq*-framework, when the frequency tends to zero (the frequency tends to fundamental frequency in $\alpha\beta$ framework), the negative resistance tends to infinity. Additionally, the previous discussions have demonstrated that the negative resistance is caused largely by the PI controller of the dc-link voltage and the integral gain of the CC. Thus, it is possible to select the small bandwidth of the DVC to shorten the negative resistor region. Since the frequency range of the LFO is normally 1–10 Hz and considering the dynamic performance, the bandwidth of dc-link voltage controller is recommended to be smaller than 5 Hz. Moreover, a higher impedance magnitude is necessary in the NRA. Alternatively, the traction network can support a part of the positive resistance that stabilizes the train-network system.

B. Recommendations

In the train-network system, a fair balance should be struck between tradeoff of weak/strong X_s/R_s grid and characters of the output impedance of the electric trains. Therefore, in order to mitigate the LFO, the following recommendations are presented.

1) Traction Network: The traction network plays an important role in the excitation of LFO. The main concern is having a strong grid that prevents LFO and other instability problems. Therefore, it is beneficial to strengthen the system to accommodate rated or higher number of electric trains that comply with the standard aforedescribed. A traction-network's SCR_t greater than 2 is recommended. In addition, while maintaining the recommended SCR_t, the X_s/R_s of the network system should be reduced by increasing the resistance of the traction network in the range of acceptable power losses.

2) Electric Trains: For the electric train, the priority should be to limit the negative resistance caused by the dc-link voltage. According to standard EN50388-2012, it requires that the electric train is passive in the frequency range above fundamental frequency. However, in (23), this goal is not attainable without a change in control technique. Therefore, to keep NRA as small as possible in the low-frequency range of 1 to 10 Hz, it is recommended that the bandwidth of the dc-link voltage PI controller is set smaller than 5 Hz.

To better avoid the LFO, more detailed design procedure should be followed. For instance, if SCR_t, the expected energized train quantity and the rated power of each train are known, the total equivalent impedance can be calculated by (36). Considering the worst-case scenario, the traction network can be regarded as pure inductance in the low-frequency range. Hence, the equivalent inductance can be expressed as

$$L_{equ}^{g} = \frac{X_s}{2\pi f_0}. \tag{40}$$

In the modified sequence domain, the impedance of the traction network is obtained as

$$Z_{pp\_\mathrm{equ}}^{g}(j\omega) = j(\omega + \omega_0)L_{equ}^{g}. \tag{41}$$

To avoid the magnitude crossover frequency of the eigenvalues in (30), the magnitude of the train impedance in the modified sequence domain should satisfy the following:

$$\left|Z_{pp}^{t}(j\omega)\right| > np\left|(\omega + \omega_0)L_{equ}^{g}\right|, \omega = 2\pi f, f \in [1\mathrm{Hz}, 10\mathrm{Hz}]. \tag{42}$$

Furthermore, (42) can be further written as

$$\left|Z_{pp}^{t}(j\omega)\right| > \max\left[np\left|(\omega + \omega_0)L_{equ}^{g}\right|\right] = np\left|120\pi L_{equ}^{g}\right|. \tag{43}$$

Therefore, the maximum value in (43) depends on the selected frequency range. For example, the worst case in Table III is $\mathrm{SCR}_t = 1.07$, where n=7 and p=10, then the equivalent inductance is approximately 0.258 mH on the secondary on-board traction transformer. When seven trains are put into service, in order to avoid intrusive negative effects, the input impedance of one 4QC should be larger than 36.6 dB in the frequency range of 1–10 Hz. This is a conservative estimate of the train impedance. Therefore, it is necessary to provide more realistic values based on industrial applications based and specifications for the ac grid-converter system [76], [77]. Moreover, accurate train-network impedance measurements [31], [78] will facilitate the impedance identification process and further development of related standards.

C. Difference From Other Stability Problems

The LFO is a type of small-signal instability issue in the power-electronics-tied grid system, behaving as a low-frequency (from 0.5 to 10 Hz) oscillation around the fundamental frequency and manifests as two coupled interharmonics $f_0 \pm f_{\mathrm{osc}}$. Moreover, similar subsynchronous oscillation and LFO have been reported in the interaction of renewable energy sources and the power grid [79]. The oscillatory conditions are similar, with a weak grid and multiple power electronic converters. The difference is the oscillatory frequency (20–70 Hz) and operation mode of the converter (inverter or rectifier). For the grid-connected inverter, the low-frequency instability is mainly caused by PLL, and the DVC causes the instability problem in low-frequency range for rectifier [70].

Another type of LFO ($<$ 3Hz) and subsynchronous oscillation ($<$ 50 Hz) occurred in the traditional power system between generators, grid (or series-capacitor compensation), and

power electronics. In addition, the generator-induced sub/super-synchronous oscillation is excited if the subsynchronous-frequency mode has a frequency that is close to a torsional mode of a remote synchronous generator in which the torsional interactions occurs [80].

The low-frequency instability occurrence also differ from the high-frequency instability around the switching frequency or Nyquist frequency (e.g., from 500 to 2500 Hz for the electric train), as a result of fast current control loop, time delay, or network harmonic resonance condition [29]. It is noteworthy that these oscillations have shared common features that are easily set-off in a weak-grid environment.

VII. Conclusion

This article discussed the phenomena, modeling, mechanism, and mitigation approaches of the LFO in the electric railway system. It has been illustrated that both the PI controller of the dc-link voltage and the integral gain of the current controller will cause negative resistance. In addition, the dc-link voltage control causes an asymmetry in the train's controller. Under weak grid or multiple-connected trains condition, the negative resistance causes LFO, and the asymmetric control structure leads to the frequency coupling.

In terms of impedance-based analysis, the design recommendations for enhancing the stability of the train-network system are summarized as follows.

1) Considering number of energized trains, SCR_t of the traction network should be ≥ 2. In addition, while maintaining the specified SCR_t, X_s/R_s ratio of the network system should be reduced by increasing the resistance of the traction network within the range of acceptable power losses.
2) The bandwidth of the dc-link voltage PI controller of the train is recommended to set < 5 Hz to reduce the negative resistance range. In addition, a conservative estimation of the magnitude limits within 1–10 Hz is also presented to avoid LFO.

References

[1] H. Hu, Y. Shao, L. Tang, J. Ma, Z. He, and S. Gao, "Overview of harmonic and resonance in railway electrification systems," *IEEE Trans. Ind. Appl.*, vol. 54, no. 5, pp. 5227–5245, Sep./Oct. 2018.

[2] H. Hu, H. Tao, F. Blaabjerg, X. Wang, Z. He, and S. Gao, "Train–network interactions and stability evaluation in high-speed railways–part I: Phenomena and modeling," *IEEE Trans. Power Electron.*, vol. 33, no. 6, pp. 4627–4642, Jun. 2018.

[3] H. Hu, H. Tao, X. Wang, F. Blaabjerg, Z. He, and S. Gao, "Train–network interactions and stability evaluation in high-speed railways—Part II: Influential factors and verifications," *IEEE Trans. Power Electron.*, vol. 33, no. 6, pp. 4643–4659, Jun. 2018.

[4] S. Danielsen, O. B. Fosso, M. Molinas, J. A. Suul, and T. T. Toftevaag, "Simplified models of a single-phase power electronic inverter for railway power system stability analysis—Development and evaluation," *Elect. Power Syst. Res.*, vol. 80, no. 2, pp. 204–214, Feb. 2010.

[5] Y. Liao, Z. Liu, H. Zhang, and B. Wen, "Low-frequency stability analysis of single-phase system with dq-frame impedance approach—Part I: Impedance modeling and verification," *IEEE Trans. Ind. Appl.*, vol. 54, no. 5, pp. 4999–5011, Sep./Oct. 2018.

[6] Y. Liao, Z. Liu, H. Zhang, and B. Wen, "Low-frequency stability analysis of single-phase system with dq-frame impedance approach—Part II: Stability and frequency analysis," *IEEE Trans. Ind. Appl.*, vol. 54, no. 5, pp. 5012–5024, Sep./Oct. 2018.

[7] F. P. Demello and C. Concordia, "Concepts of synchronous machine stability as affected by excitation control," *IEEE Trans. Power App. Syst.*, vol. 88, no. 4, pp. 316–329, Apr. 1969.

[8] H. Wang, M. Wu, and J. Sun, "Analysis of low-frequency oscillation in electric railways based on small-signal modeling of vehicle-grid system in dq frame," *IEEE Trans. Power Electron.*, vol. 30, no. 9, pp. 5318–5330, Sep. 2015.

[9] S. B. Carlos, "Direct generation of low frequency single phase AC for the railway in Norway and Sweden," Ph.D. dissertation, Royal Inst Technol., Stockholm, Sweden, 2009.

[10] M. M. Steinar Danielsen, T. Toftevaag, and O. B. Fosso, "Constant power load characteristic's influence on the low-frequency interaction between advanced electrical rail vehicle and railway traction power supply with rotary converters," in *Proc. Modern Elect. Traction 9th Int. Conf.*, Sep. 2009, pp. 1–6.

[11] S. Danielsen, "Electric traction power system stability," Ph.D. dissertation, Univ. Sci.Technol., Norwegian, 2010.

[12] D. Frugier and P. Ladoux, "Voltage disturbances on 25kV-50 Hz railway lines – Modelling method and analysis," in *Proc. Int. Symp. Power Electron. Elect. Drives Autom. Motion*, Jun. 2010, pp. 1080–1085.

[13] X. Jiang *et al.*, "Study on low-frequency voltage fluctuation of traction power supply system introduced by multiple modern trains," *Elect. Power Syst. Res.*, vol. 146, pp. 246–257, May 2017.

[14] L. Jing and M. Wu, "Measurement and analysis on low-frequency oscillation in Xuzhou electrical railway hub," in *Proc. Int. Conf. Elect. Inf. Technol. Rail Transp.*, Mar. 2016, pp. 659–666.

[15] C. Heising, R. Bartelt, M. Oettmeier, V. Staudt, and A. Steimel, "Enhancement of low-frequency system stability of 60-Hz railway power grids," in *Proc. 14th Int. Power Electron. Motion Control Conf.*, Sep. 2010, pp. S7-1–S7-8.

[16] H. Y. Assefa, S. Danielsen, and M. Molinas, "Impact of PWM switching on modeling of low frequency power oscillation in electrical rail vehicle," in *Proc. 13th Eur. Conf. Power Electron. Appl.*, Sep. 2009, pp. 1–9.

[17] R. Bartelt, M. Oettmeier, C. Heising, and V. Staudt, "Advanced simulation concept for interaction of railway grid representation and model power train of AC locomotive," in *Proc. Int. Conf. Power Eng., Energy. Elect. Drives*, Mar. 2009, pp. 267–272.

[18] K. Jiang, C. Zhang, and X. Ge, "Low-frequency oscillation analysis of the train-grid system based on an improved forbidden-region criterion," *IEEE Trans. Ind. Appl.*, vol. 54, no. 5, pp. 5064–5073, Sep./Oct. 2018.

[19] Y. Liao, Z. Liu, G. Zhang, and C. Xiang, "Vehicle-grid system modeling and stability analysis with forbidden region-based criterion," *IEEE Trans. Power Electron.*, vol. 32, no. 5, pp. 3499–3512, May 2017.

[20] Y. Hong, Z. Shuai, H. Cheng, C. Tu, Y. Li, and Z. J. Shen, "Stability analysis of low-frequency oscillation in train-network system using RLC circuit model," *IEEE Trans. Transp. Electrific.*, vol. 5, no. 2, pp. 502–514, Jun. 2019.

[21] Y. Zhou, H. Hu, X. Yang, J. Yang, Z. He, and S. Gao, "Low frequency oscillation traceability and suppression in railway electrification systems," *IEEE Trans. Ind. Appl.*, vol. 55, no. 6, pp. 7699–7711, Nov./Dec. 2019.

[22] Y. Mishra, S. Mishra, F. Li, Z. Y. Dong, and R. C. Bansal, "Small-signal stability analysis of a DFIG-based wind power system under different modes of operation," *IEEE Trans. Energy Convers.*, vol. 24, no. 4, pp. 972–982, Dec. 2009.

[23] Y. Wang, X. Wang, F. Blaabjerg, and Z. Chen, "Harmonic instability assessment using state-space modeling and participation analysis in inverter-fed power systems," *IEEE Trans. Ind. Electron.*, vol. 64, no. 1, pp. 806–816, Jan. 2017.

[24] Y. Wang, X. Wang, Z. Chen, and F. Blaabjerg, "Small-signal stability analysis of inverter-fed power systems using component connection method," *IEEE Trans. Smart Grid*, vol. 9, no. 5, pp. 5301–5310, Sep. 2018.

[25] R. D. Middlebrook, "Input filter considerations in design and application of switching regulators," in *Proc. IEEE Ind. Appl. Soc. Annu. Meeting*, Oct. 1976, pp. 366–382.

[26] J. Sun, "Impedance-based stability criterion for grid-connected inverters," *IEEE Trans. Power Electron.*, vol. 26, no. 11, pp. 3075–3078, Nov. 2011.

[27] H. Tao, H. Hu, X. Wang, F. Blaabjerg, and Z. He, "Impedance-based harmonic instability assessment in a multiple electric trains and traction network interaction system," *IEEE Trans. Ind. Appl.*, vol. 54, no. 5, pp. 5083–5096, Sep./Oct. 2018.

[28] M. Amin and M. Molinas, "Small-signal stability assessment of power electronics based power systems: A discussion of impedance- and eigenvalue-based methods," *IEEE Trans. Ind. Appl.*, vol. 53, no. 5, pp. 5014–5030, Sep./Oct. 2017.

[29] X. Wang and F. Blaabjerg, "Harmonic stability in power electronic-based power systems: Concept, modeling, and analysis," *IEEE Trans. Smart Grid*, vol. 10, no. 3, pp. 2858–2870, May 2019.

[30] J. Sun, "Small-signal methods for AC distributed power systems–a review," *IEEE Trans. Power Electron.*, vol. 24, no. 11, pp. 2545–2554, Nov. 2009.

[31] P. Pan, H. Hu, X. Yang, F. Blaabjerg, X. Wang, and Z. He, "Impedance measurement of traction network and electric train for stability analysis in high-speed railways," *IEEE Trans. Power Electron.*, vol. 33, no. 12, pp. 10086–10100, Dec. 2018.

[32] L. Harnefors, M. Bongiorno, and S. Lundberg, "Input-admittance calculation and shaping for controlled voltage-source converters," *IEEE Trans. Ind. Electron.*, vol. 54, no. 6, pp. 3323–3334, Dec. 2007.

[33] J. Kwon, X. Wang, F. Blaabjerg, C. L. Bak, A. R. Wood, and N. R. Watson, "Linearized modeling methods of AC–DC converters for an accurate frequency response," *IEEE J. Emerg. Sel. Topics Power Electron.*, vol. 5, no. 4, pp. 1526–1541, Dec. 2017.

[34] J. B. Kwon, X. Wang, F. Blaabjerg, C. L. Bak, A. R. Wood, and N. R. Watson, "Harmonic instability analysis of a single-phase grid-connected converter using a harmonic state-space modeling method," *IEEE Trans. Ind. Appl.*, vol. 52, no. 5, pp. 4188–4200, Sep./Oct. 2016.

[35] B. Wen, D. Boroyevich, R. Burgos, P. Mattavelli, and Z. Shen, "Analysis of D-Q small-signal impedance of grid-tied inverters," *IEEE Trans. Power Electron.*, vol. 31, no. 1, pp. 675–687, Jan. 2016.

[36] J. Sun, Z. Bing, and K. J. Karimi, "Input impedance modeling of multipulse rectifiers by harmonic linearization," *IEEE Trans. Power Electron.*, vol. 24, no. 12, pp. 2812–2820, Dec. 2009.

[37] G. C. Verghese and V. J. Thottuvelil, "Aliasing effects in PWM power converters," in *Proc. 30th Annu. IEEE Power Electron. Specialists Conf. Rec.*, Jul. 1999, vol. 2, pp. 1043–1049.

[38] X. Wang, L. Harnefors, and F. Blaabjerg, "Unified impedance model of grid-connected voltage-source converters," *IEEE Trans. Power Electron.*, vol. 33, no. 2, pp. 1775–1787, Feb. 2018.

[39] H. Wang, " Research on the electrical low-frequency oscillation in the vehicle-grid system of electric railways," Ph.D. dissertation, Beijing Jiaotong Univ., Beijing, China, 2015, (In Chinese).

[40] J. Yao, M. Liu, C. Li, and Q. Li, "Harmonics and reactive power of power transformers with DC bias," in *Proc. Asia Pacific Power Energy Eng. Conf.*, 2010, pp. 1–4.

[41] M. Wu, C. Roberts, and S. Hillmansen, "Modelling of AC feeding systems of electric railways based on a uniform multi-conductor chain circuit topology," in *Proc. IET Conf. Railway Traction Syst.*, Apr. 2010, pp. 1–5.

[42] M. Wu, "Study on electrical parameters and mathematical model of traction power supply system," Ph.D. dissertation, Beijing Jiaotong Univ., Beijing, China, 2006, (in Chinese).

[43] V. Blahnik, T. Kosan, and J. Talla, "Control of single-phase AC/DC converter based on SOGI-PLL voltage synchronization," in *Proc. 16th Int. Conf. Mechatronics - Mechatronika*, 2014, pp. 652–655.

[44] Y. Gui, M. Li, J. Lu, S. Golestan, J. M. Guerrero, and J. C. Vasquez, "A voltage modulated DPC approach for three-phase PWM rectifier," *IEEE Trans. Ind. Electron.*, vol. 65, no. 10, pp. 7612–7619, Oct. 2018.

[45] P. Wang, H. Li, T. Cao, X. Wang and J. Xu, "Proof of equivalence between two interlaced two-level PWM rectifiers and three-level PWM rectifiers," *J. China Railway Soc.*, vol. 41, p. 6, Jan. 2019, (in Chinese).

[46] D. Yang, X. Wang, and F. Blaabjerg, "Sideband harmonic instability of paralleled inverters with asynchronous carriers," *IEEE Trans. Power Electron.*, vol. 33, no. 6, pp. 4571–4577, Jun. 2018.

[47] S. Golestan, J. M. Guerrero, and J. C. Vasquez, "Single-phase PLLs: A review of recent advances," *IEEE Trans. Power Electron.*, vol. 32, no. 12, pp. 9013–9030, Dec. 2017.

[48] H. Liu, X. Xie, X. Gao, H. Liu, and Y. Li, "Stability analysis of SSR in multiple wind farms connected to series-compensated systems using impedance network model," *IEEE Trans. Power Syst.*, vol. 33, no. 3, pp. 3118–3128, May 2018.

[49] H. Liu and X. Xie, "Impedance network modeling and quantitative stability analysis of sub-/super-synchronous oscillations for large-scale wind power systems," *IEEE Access*, vol. 6, pp. 34431–34438, 2018.

[50] W. Cao, Y. Ma, L. Yang, F. Wang, and L. M. Tolbert, "D-Q impedance based stability analysis and parameter design of three-phase inverter-based AC power systems," *IEEE Trans. Ind. Electron.*, vol. 64, no. 7, pp. 6017–6028, Jul. 2017.

[51] A. Rygg, M. Molinas, C. Zhang, and X. Cai, "A modified sequence-domain impedance definition and its equivalence to the dq-domain impedance definition for the stability analysis of AC power electronic systems," *IEEE J. Emerg. Sel. Topics Power Electron.*, vol. 4, no. 4, pp. 1383–1396, Dec. 2016.

[52] A. Rygg, M. Molinas, C. Zhang, and X. Cai, "On the equivalence and impact on stability of impedance modeling of power electronic converters in different domains," *IEEE J. Emerg. Sel. Topics Power Electron.*, vol. 5, no. 4, pp. 1444–1454, Dec. 2017.

[53] B. Wen, R. Burgos, D. Boroyevich, P. Mattavelli, and Z. Shen, "AC stability analysis and dq frame impedance specifications in power-electronics-based distributed power systems," *IEEE J. Emerg. Sel. Topics Power Electron.*, vol. 5, no. 4, pp. 1455–1465, Dec. 2017.

[54] Y. Zhou, H. Hu, P. Pan, and Z. He, "Impedance specification and stability analysis for the AC grid-converter system in modified sequence-domain," *IFAC Papersonline*, vol. 52, no. 4, pp. 188–193, 2019.

[55] C. M. Wildrick, F. C. Lee, B. H. Cho, and B. Choi, "A method of defining the load impedance specification for a stable distributed power system," *IEEE Trans. Power Electron.*, vol. 10, no. 3, pp. 280–285, May 1995.

[56] L. Harnefors, A. G. Yepes, A. Vidal, and J. Doval-Gandoy, "Passivity-based controller design of grid-connected VSCs for prevention of electrical resonance instability," *IEEE Trans. Ind. Electron.*, vol. 62, no. 2, pp. 702–710, Feb. 2015.

[57] D. Lu, X. Wang, and F. Blaabjerg, "Impedance-based analysis of DC-link voltage dynamics in voltage-source converters," *IEEE Trans. Power Electron.*, vol. 34, no. 4, pp. 3973–3985, Apr. 2019.

[58] A. Yogarathinam, J. Kaur, and N. R. Chaudhuri, "Impact of inertia and effective short circuit ratio on control of frequency in weak grids interfacing LCC-HVDC and DFIG-based wind farms," *IEEE Trans. Power Del.*, vol. 32, no. 4, pp. 2040–2051, Aug. 2017.

[59] Z. Liu, X. Hu, and Y. Liao, "Vehicle-grid system stability analysis based on norm criterion and suppression of low-frequency oscillation with MMC-STATCOM," *IEEE Trans. Transp. Electrific.*, vol. 4, no. 3, pp. 757–766, Sep. 2018.

[60] S. Wu, Z. Liu, and H. Zhang, "Suppression of low-frequency oscillation with cascaded H-bridge multi-level active power filter in vehicle-grid system," in *Proc. IEEE Student Conf. Elect. Mach. Syst.*, Dec. 2018, pp. 1–5.

[61] X. Jiang, H. Hu, X. Yang, Z. He, Q. Qian, and P. Tricoli, "Analysis and adaptive mitigation scheme of low-frequency oscillations in AC railway traction power systems," *IEEE Trans. Transp. Electrific.*, vol. 5, no. 3, pp. 715–726, Sep. 2019.

[62] H. Hu, Y. Zhou, J. Yang, Z. He, and S. Gao, "A practical approach to mitigate low-frequency oscillation in railway electrification systems," *IEEE Trans. Power Electron.*, vol. 33, no. 10, pp. 8198–8203, Oct. 2018.

[63] G. Zhang, Z. Liu, S. Yao, Y. Liao, and C. Xiang, "Suppression of low-frequency oscillation in traction network of high-speed railway based on auto-disturbance rejection control," *IEEE Trans. Transp. Electrific.*, vol. 2, no. 2, pp. 244–255, Jun. 2016.

[64] H. Bai *et al.*, "Passivity enhancement of grid-tied converters by series LC-filtered active damper," *IEEE Trans. Ind. Electron.*, vol. 64, no. 1, pp. 369–379, Jan. 2017.

[65] L. Wang, C. Chang, B. Kuan, and A. V. Prokhorov, "Stability improvement of a two-area power system connected with an integrated onshore and offshore wind farm using a STATCOM," *IEEE Trans. Ind. Appl.*, vol. 53, no. 2, pp. 867–877, Mar.–Apr. 2017.

[66] K. R. Padiyar and N. Prabhu, "Design and performance evaluation of subsynchronous damping controller with STATCOM," *IEEE Trans. Power Del.*, vol. 21, no. 3, pp. 1398–1405, Jul. 2006.

[67] Z. Shuai, H. Cheng, J. Xu, C. Shen, Y. Hong, and Y. Li, "A notch filter based active damping control method for low frequency oscillation suppression in train-network interaction systems," *IEEE J. Emerg. Sel. Topics Power Electron.*, vol. 7, no. 4, pp. 2417–2427, Dec. 2019.

[68] X. Zhang, X. Ruan, and Q. Zhong, "Improving the stability of cascaded DC/DC converter systems via shaping the input impedance of the load converter with a parallel or series virtual impedance," *IEEE Trans. Ind. Electron.*, vol. 62, no. 12, pp. 7499–7512, Dec. 2015.

[69] X. Wang, Y. W. Li, F. Blaabjerg, and P. C. Loh, "Virtual-impedance-based control for voltage-source and current-source converters," *IEEE Trans. Power Electron.*, vol. 30, no. 12, pp. 7019–7037, Dec. 2015.

[70] L. Harnefors, X. Wang, A. G. Yepes, and F. Blaabjerg, "Passivity-based stability assessment of grid-connected VSCs—An overview," *IEEE J. Emerg. Sel. Topics Power Electron.*, vol. 4, no. 1, pp. 116–125, Mar. 2016.

[71] J. Siegers, S. Arrua, and E. Santi, "Stabilizing controller design for multi-bus MVdc distribution systems using a passivity-based stability criterion and positive feedforward control," *IEEE J. Emerg. Sel. Topics Power Electron.*, vol. 5, no. 1, pp. 14–27, Mar. 2017.
[72] Z. Liu, Y. Wang, S. Liu, Z. Li, H. Zhang, and Z. Zhang, "An approach to suppress low-frequency oscillation by combining extended state observer with model predictive control of EMUs rectifier," *IEEE Trans. Power Electron.*, vol. 34, no. 10, pp. 10282–10297, Oct. 2019.
[73] Z. Liu, Z. Geng, and X. Hu, "An approach to suppress low frequency oscillation in the traction network of high-speed railway using passivity-based control," *IEEE Trans. Power Syst.*, vol. 33, no. 4, pp. 3909–3918, Jul. 2018.
[74] BS EN 50388: 2012, "Railway Applications —Power supply and rolling stock — Technical criteria for the coordination between power supply (substation) and rolling stock to achieve interoperability," BSI Standards Publication, Aug. 2012.
[75] I. Pendharkar, "Resonance stability in electrical railway systems—A dissipativity approach," in *Proc. Eur. Control Conf.*, Jul. 2013, pp. 4574–4579.
[76] Z. Liu, J. Liu, W. Bao, and Y. Zhao, "Infinity-norm of impedance-based stability criterion for three-phase AC distributed power systems with constant power loads," *IEEE Trans. Power Electron.*, vol. 30, no. 6, pp. 3030–3043, Jun. 2015.
[77] Y. Zhou, H. Hu, J. Yang, and Z. He, "A novel forbidden-region-based stability criterion in modified sequence-domain for AC grid-converter system," *IEEE Trans. Power Electron.*, vol. 34, no. 4, pp. 2988–2995, Apr. 2019.
[78] H. Hu, P. Pan, Y. Song, and Z. He, "A novel controlled frequency band impedance measurement approach for single-phase railway traction power system," *IEEE Trans. Ind. Electron.*, vol. 67, no. 1, pp. 244–253, Jan. 2020.
[79] H. Liu *et al.*, "Subsynchronous interaction between direct-drive PMSG based wind farms and weak AC networks," *IEEE Trans. Power Syst.*, vol. 32, no. 6, pp. 4708–4720, Nov. 2017.
[80] Y. Li, L. Fan, and Z. Miao, "Wind in weak grids: Low-frequency oscillations, subsynchronous oscillations, and torsional interactions," *IEEE Trans. Power Syst.*, vol. 35, no. 1, pp. 109–118, Jan. 2010.

Haitao Hu (Senior Member, IEEE) received the B.S. degree from Zhengzhou University, Zhengzhou, China, in 2010, and the Ph.D. degree from Southwest Jiaotong University, Chengdu, China, in 2014, all in electrical engineering.

From 2013 to 2014, he worked as a Visiting Doctoral Scholar at the University of Alberta, Edmonton, Canada. He is currently a Professor with School of Electrical Engineering, Southwest Jiaotong University, Chengdu, China. His main research interests include power quality and stability of the electric traction systems.

Yi Zhou (Student Member, IEEE) received the B.S. degree in electrical engineering in 2016 from Southwest Jiaotong University, Chengdu, China, where he is currently working toward the Ph.D. degree in electrical engineering.

His research interests include modeling and control of the high-speed train, stability analysis, and control of power electronic based power systems.

Xin Li received the B.S. degree in electrical engineering in 2018 from Southwest Jiaotong University, Chengdu, China, where she is currently working toward the master's degree in electrical engineering.

Her research interests include the modeling and stability analysis of the high-speed train-network systems.

Ke Lei received the B.S. degree in electrical engineering from East China Jiaotong University, Nanchang, China, in 2018. He is currently working toward the master's degree in electrical engineering with Southwest Jiaotong University, Chengdu, China.

His research interests mainly include the stability of traction power supply systems, harmonic analysis, and harmonic detection algorithms.